



Supplement of

Aerosol characterization over the southeastern United States using high-resolution aerosol mass spectrometry: spatial and seasonal variation of aerosol composition and sources with a focus on organic nitrates

L. Xu et al.

Correspondence to: N. L. Ng (ng@chbe.gatech.edu)

The copyright of individual parts of the supplement might differ from the CC-BY 3.0 licence.

24 The selection of optimal solutions for PMF analysis on merged organic and nitrate mass
25 spectra (i.e., $\text{PMF}_{\text{org+NO}_3}$) is mainly based on comparing the time series (Fig. S5), mass spectrum
26 (Fig. S5), and campaign-average mass concentration (Fig. S6) with factors from PMF analysis on
27 organic mass spectra only (i.e., PMF_{org}), in addition to examining the typical diagnostic plots
28 (Fig. S3). Based on the identification of a nitrate inorganic aerosol (NIA) factor, we divide all
29 seven datasets into two categories: 1) CTR_June and YRK_July where a NIA factor is not
30 resolved and 2) the other sites where a NIA factor is resolved.

31 For CTR_June and YRK_July, the same factors are resolved from $\text{PMF}_{\text{org+NO}_3}$ analysis as
32 those from PMF_{org} analysis. The factors from $\text{PMF}_{\text{org+NO}_3}$ show good correlation with
33 corresponding factors from PMF_{org} regarding both time series ($R>0.964$) and mass spectrum
34 ($R>0.997$) (Fig. S5).

35 We note that in the optimal solutions of CTR_June and YRK_July, the residuals of NO^+
36 and NO_2^+ (i.e., $\sum(\text{Resid}^2/\sigma^2)/Q_{\text{exp}}$) are larger than that in the optimal solutions of other sites
37 where NIA factor is resolved (Fig. S3). If one goes to higher number factor solutions, the
38 residuals of NO^+ and NO_2^+ of CTR_June and YRK_July are reduced, but the correlations
39 between factors from $\text{PMF}_{\text{Org+NO}_3}$ and corresponding factors from PMF_{Org} are weakened and
40 splitting behavior of real factors occurs (Ulbrich et al., 2009). Take YRK_July for example, the
41 residual of NO^+ decreases from 155 in the three-factor solution (Fig. S3(c)) to 31 in the five-
42 factor solution (Fig. S16). However, the correlations of the time series between factors from
43 $\text{PMF}_{\text{Org+NO}_3}$ and the corresponding factors from PMF_{Org} are all weakened (Fig. S17 and S5). In
44 addition, MO-OOA in three-factor solution splits into two factors in five-factor solution. Thus,
45 we select three-factor solution as the optimal solution for YRK_July in the $\text{PMF}_{\text{Org+NO}_3}$ analysis.

46 For all the sites except CTR_June and YRK_July, a nitrate inorganic aerosol (NIA) factor
47 was resolved. All OA factors except LO-OOA from $\text{PMF}_{\text{org+NO}_3}$ show good correlation with the
48 corresponding PMF_{org} OA factors with $R>0.89$ for time series and $R>0.98$ for mass spectrum
49 (Fig. S5). The correlation of the LO-OOA time series obtained from $\text{PMF}_{\text{org+NO}_3}$ and PMF_{org}
50 analysis ranges from 0.77 to 0.98 (Fig. S5), which is not as strong as the correlation of other OA
51 factors. This is likely due to that the time series of LO-OOA being more similar to the total
52 measured nitrate (i.e., $\text{NO}_{3,\text{meas}}$) than other OA factors, so that PMF has difficulty in separating
53 LO-OOA and NIA factor.

54 An FPEAK value of 0 is chosen for all datasets except RS_Jan. For RS_Jan dataset,
55 PMF_{org+NO₃} solution with FPEAK = 0.2 is selected due to the following reasons. First of all,
56 solution with FPEAK=0 is not converged. Second of all, solution with FPEAK = 0.2 provides
57 the best correlation with PMF_{org} factors for all the OA factors from PMF_{org+NO₃} analysis. For
58 example, PMF_{org+NO₃} solution with FPEAK =-0.2 cannot resolve a clear LO-OOA factor as
59 shown in Fig. S18.

60 Unlike all the other sites where all PMF_{org} OA factors can be clearly resolved in the
61 corresponding PMF_{org+NO₃} analysis, we cannot resolve MO-OOA factor from PMF_{org+NO₃} for
62 YRK_Dec even up to ten-factor solution. From PMF_{org} analysis on YRK_Dec, we resolved three
63 factors, which are MO-OOA, LO-OOA, and BBOA. For PMF_{org+NO₃} on YRK_Dec, in the two-
64 factor solution, we resolve one NIA factor and only one OA factor, indicating that a two-factor
65 solution is insufficient to separate BBOA and OOA factors. In the three-factor solution, we
66 resolve clear NIA and BBOA factors, but just one OOA factor. This OOA factor correlates well
67 with the combined LO-OOA and MO-OOA factors from PMF_{org} three-factor solution ($R=0.94$)
68 (Fig. S19(b)), indicating the OOA factor from PMF_{org+NO₃} three-factor solution likely represents
69 the combination of LO-OOA and MO-OOA from PMF_{org} three-factor solution. In PMF_{org+NO₃}
70 four-factor solution, we resolve a factor whose correlation with all factors from PMF_{org} is very
71 weak (i.e., the highest R is 0.63) (Fig. S19(c)). This suggests that “splitting” behavior occurs for
72 the PMF_{org+NO₃} four-factor solution. Taken together, PMF_{org+NO₃} with a three-factor solution is
73 optimal for YRK_Dec. It is also important to note that the focus of PMF_{org+NO₃} is for nitrate
74 source apportionment. Although PMF_{org+NO₃} resolves different OA factors for different solutions,
75 the concentration of the NIA factor remains almost constant (i.e., the NIA factor concentration
76 ranges from 0.54 - 0.6 $\mu\text{g}/\text{m}^3$ from 2 to 5 factor solutions). Thus, the number of factors resolved
77 for YRK_Dec has minimal effect on our conclusion.

78

79

80

81

82

83 **Figure Captions**

84

85 Fig. S1. Diagnostic plots of the PMF analysis on the high-resolution organic mass spectra (i.e.,
86 PMF_{org}). The following plots are shown for all the datasets: (1) Q/Q_{exp} vs number of factors; (2)
87 Q/Q_{exp} vs. FPEAK for the solution with optimal number of factors; (3) mass fraction of PMF
88 factors vs. FPEAK; (4) correlations of time series and mass spectra among PMF factors; (5) the
89 distribution of scaled residuals for each m/z; (6) the time series of the measured and the
90 reconstructed organic mass; (7) variations of the residual (= measured - reconstructed) of the
91 least-square-fit vs. time; (8) the time series of Q/Q_{exp} ; (9) the Q/Q_{exp} values vs. m/z .

92 Fig. S2. Mass spectra and time series of OA factors resolved from PMF analysis on the high-
93 resolution organic mass spectra (i.e. PMF_{org} analysis). Mass spectra are colored by ion type. The
94 time series of independent external tracers are also included.

95 Fig. S3. Diagnostic plots of the PMF analysis on the high-resolution merged organic and nitrate
96 mass spectra (i.e. $\text{PMF}_{\text{org+NO}_3}$ analysis). The following plots are shown for all the datasets: (1)
97 Q/Q_{exp} vs. number of factors; (2) Q/Q_{exp} vs FPEAK for the solution with optimal number of
98 factors; (3) mass fraction of PMF factors vs. FPEAK; (4) correlations of time series and mass
99 spectra among PMF factors; (5) the distribution of scaled residuals for each m/z; (6) the time
100 series of the measured and the reconstructed organic mass; (7) variations of the residual (=
101 measured - reconstructed) of the least-square-fit vs. time; (8) the time series of Q/Q_{exp} ; (9) the
102 Q/Q_{exp} values vs. m/z .

103 Fig. S4. Mass spectra of OA factors resolved from PMF analysis on the high-resolution merged
104 organic and nitrate mass spectra (i.e. $\text{PMF}_{\text{org+NO}_3}$ analysis). Mass spectra are colored by ion type.

105 Fig. S5. Comparison between factors resolved from PMF analysis on merged organic and nitrate
106 mass spectra (i.e. $\text{PMF}_{\text{org+NO}_3}$) and factors resolved from PMF analysis on organic mass spectra
107 (i.e. PMF_{org}) for all datasets. Each sub-panel shows the correlation coefficients of each factor
108 from $\text{PMF}_{\text{org+NO}_3}$ against all factors from PMF_{org} in terms of either mass spectrum or time series.
109 The factors from $\text{PMF}_{\text{org+NO}_3}$ are color-coded in the same way as Fig. S10, that is, MO-OOA, LO-
110 OOA, Isoprene-OA, HOA, BBOA, COA are dark green, light green, blue, grey, brown, and
111 yellow, respectively.

112 Fig. S6. The comparison of campaign-averaged mass concentration of factors resolved from
113 PMF analysis on merged organic and nitrate mass spectra (i.e. $\text{PMF}_{\text{org+NO}_3}$) and factors resolved
114 from PMF analysis on organic mass spectra (i.e. PMF_{org}). RIE and CE are not applied.

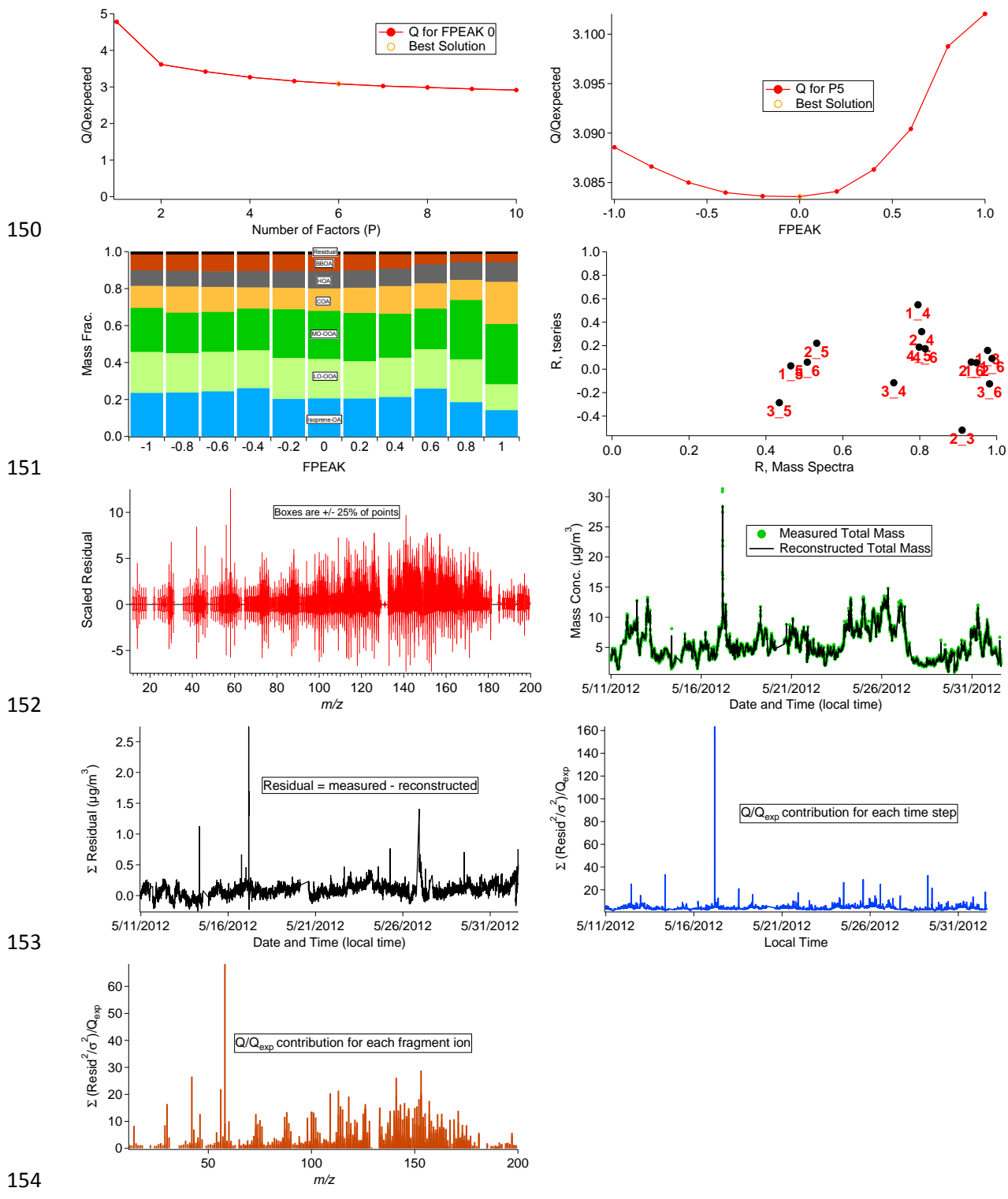
115 Fig. S7. Campaign-averaged mass spectra of total OA for all datasets. Mass spectra are colored
116 by ion type.

117 Fig. S8. Diurnal profiles of brown carbon light absorption for all the datasets.

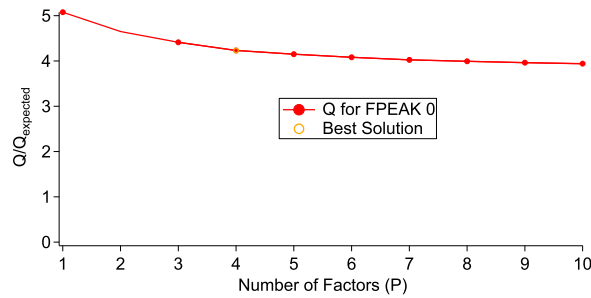
- 118 Fig. S9. Scatter plot of Isoprene-OA vs. brown carbon light absorption for the datasets where a
119 Isoprene-OA factor was resolved.
- 120 Fig. S10. The atomic O:C and H:C ratios of OA factors resolved from PMF analysis on high-
121 resolution organic mass spectra (i.e. PMF_{org}).
- 122 Fig. S11. Mass fractions of nitrate signals (i.e., NO^+ and NO_2^+) and organic signals in the nitrate
123 inorganic aerosol (NIA) factor for the datasets where a NIA factor was resolved.
- 124 Fig. S12. $\text{NO}^+/\text{NO}_2^+$ ratio of the nitrate inorganic aerosol (NIA) factor resolved from PMF
125 analysis on merged organic and nitrate mass spectra (i.e. $\text{PMF}_{\text{org+NO}_3}$ analysis). The y-axis is
126 normalized by the $\text{NO}^+/\text{NO}_2^+$ ratio of ammonium nitrate of each dataset.
- 127 Fig. S13. Time series of sodium and nitrate measured by a PILS-IC at Centreville, AL. The
128 $\text{PM}_{2.5}$ cyclone was replaced with a PM_1 cyclone on June 24th, 2013.
- 129 Fig. S14. The comparison between ACSM measurements (stationary at the Georgia Tech site)
130 and HR-ToF-AMS measuremens (rotating among different sites) of NR- PM_1 species.
- 131 Fig. S15. Diurnal profiles of $R_{\text{meas}}/R_{\text{AN}}$ for all datasets.
- 132 Fig. S16. The Q/Q_{exp} values for each m/z in the five-factor solution of $\text{PMF}_{\text{org+NO}_3}$ analysis on the
133 YRK_July dataset.
- 134 Fig. S17. Correlation coefficients of the time series of factors from $\text{PMF}_{\text{org+NO}_3}$ (five-factor
135 solution) with the time series of factors from PMF_{org} (three-factor solution) for YRK_July.
- 136 Fig. S18. Correlation coefficients of the time series of factors from $\text{PMF}_{\text{org+NO}_3}$ (six-factor
137 solution with FPEAK = -0.2) with the time series of factors from PMF_{org} (five-factor solution for
138 RS_Jan).
- 139 Fig. S19. Correlation coefficients of the time series of factors from $\text{PMF}_{\text{org+NO}_3}$ (from two-factor
140 solution to four-factor solution) with the time series of factors from PMF_{org} (three-factor solution
141 for YRK_Dec).
- 142
- 143
- 144
- 145
- 146
- 147

148 Fig. S1.

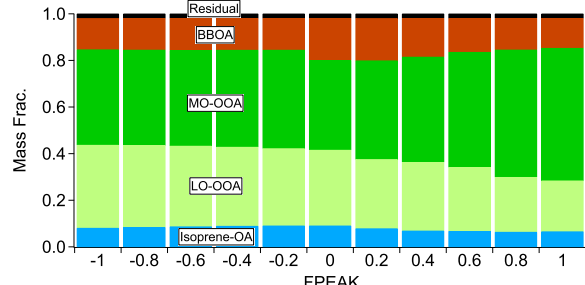
149 a) JST_May



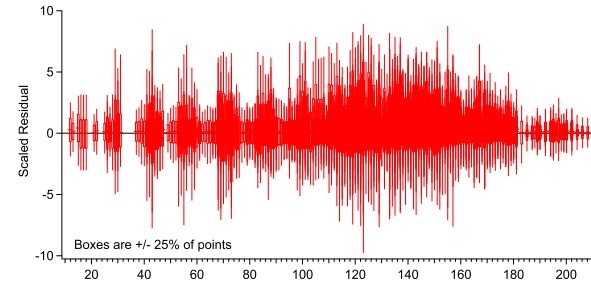
156 b) CTR_June



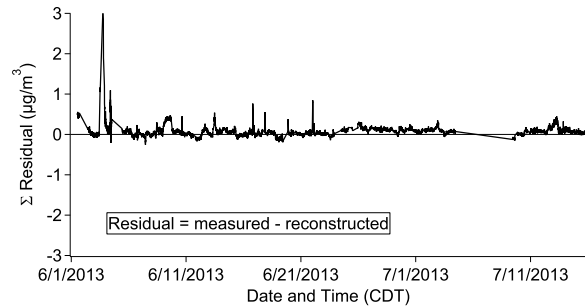
157



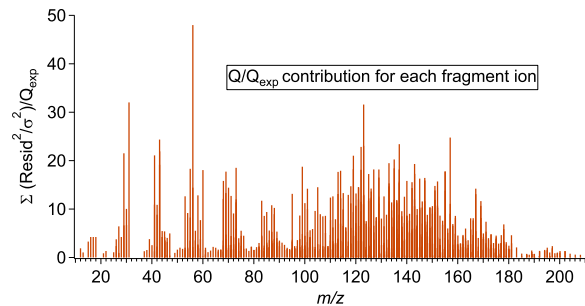
158



159

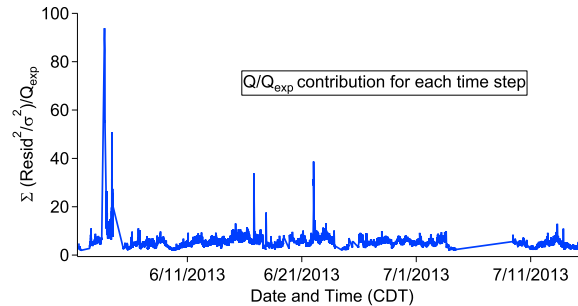
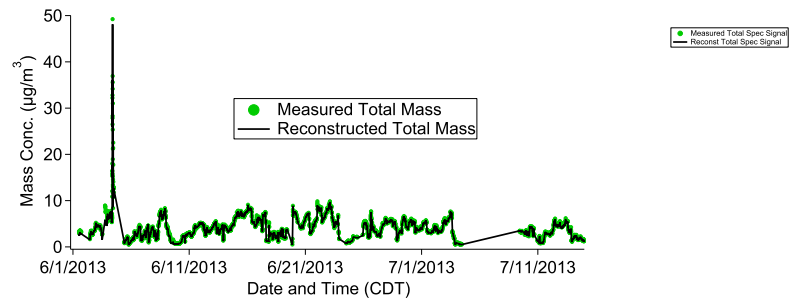
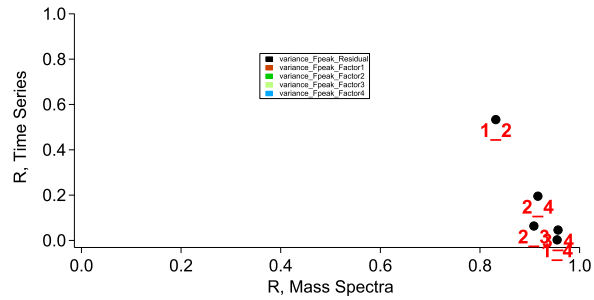
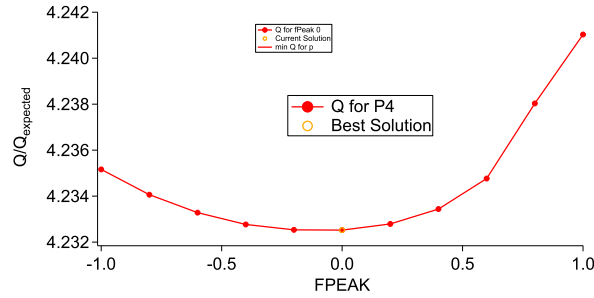


160

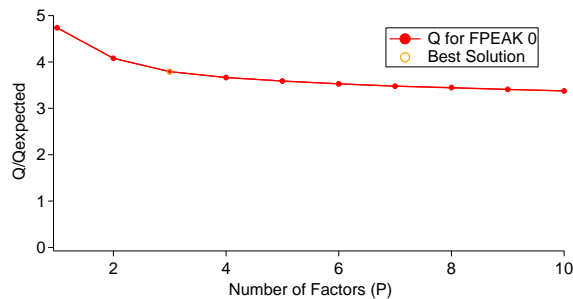


161

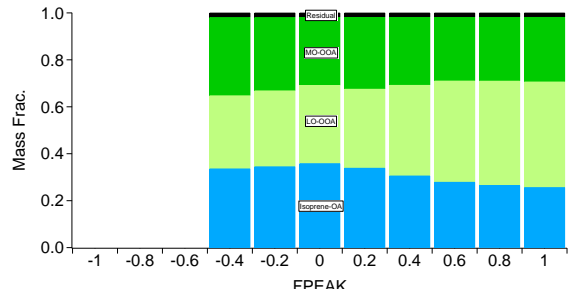
162



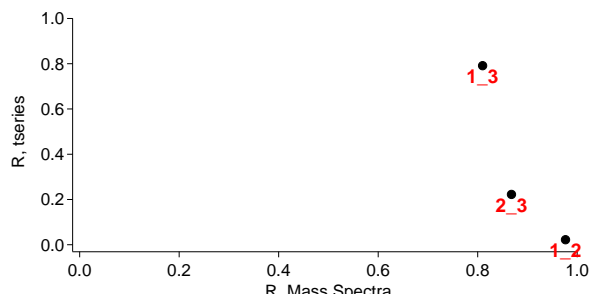
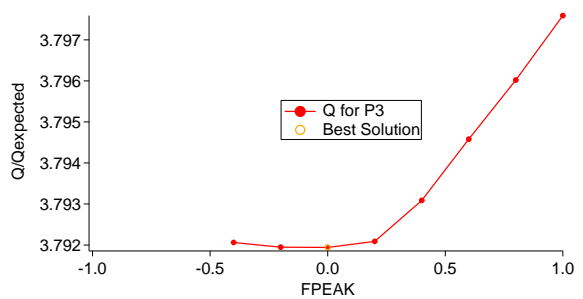
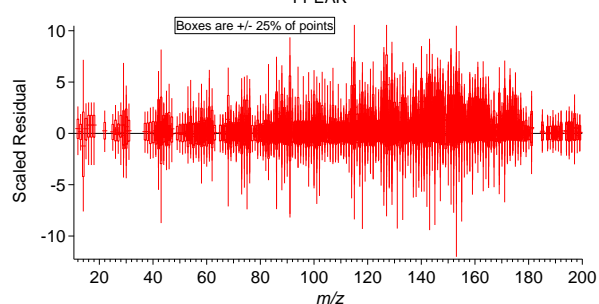
163 c) YRK_July



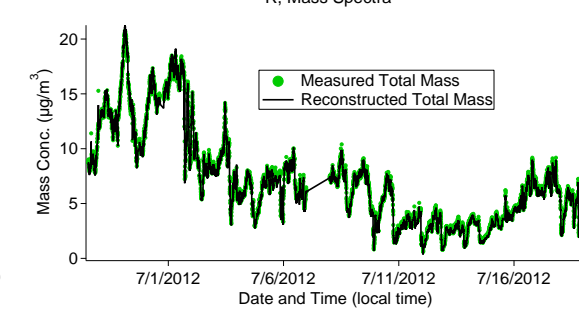
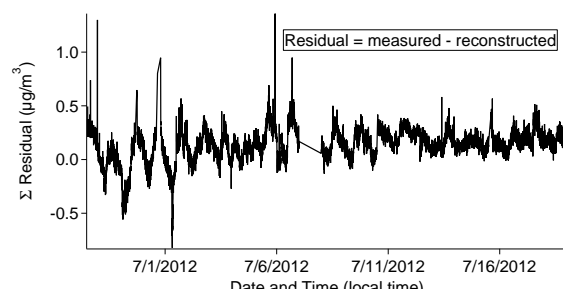
164



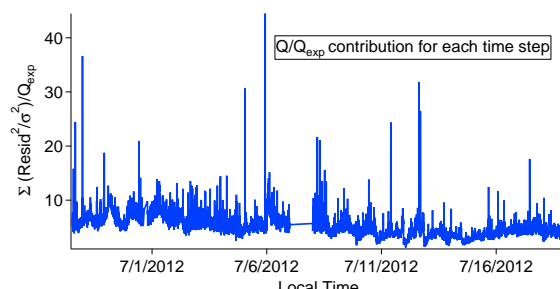
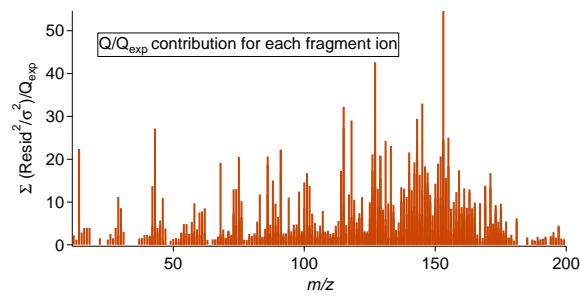
165



166



167

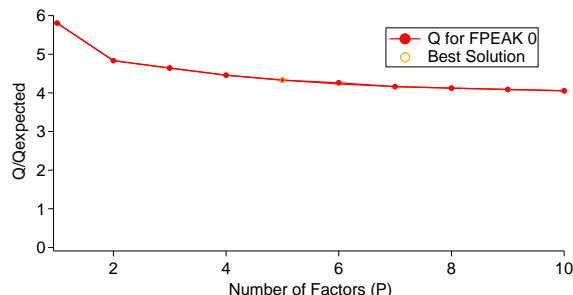


168

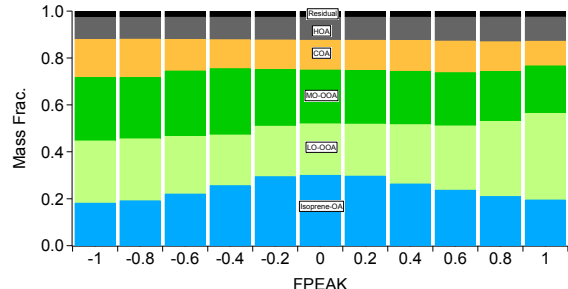
169

170

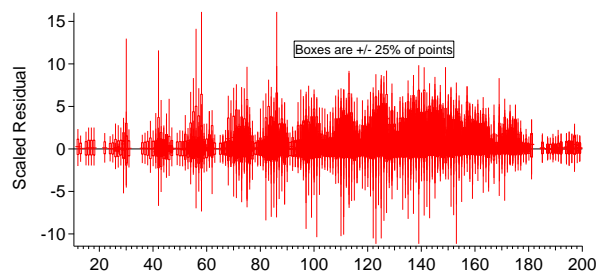
171 d) GT_Aug



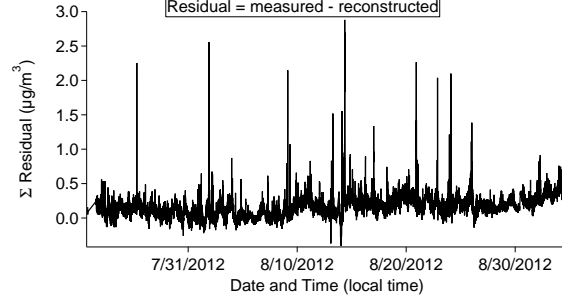
172



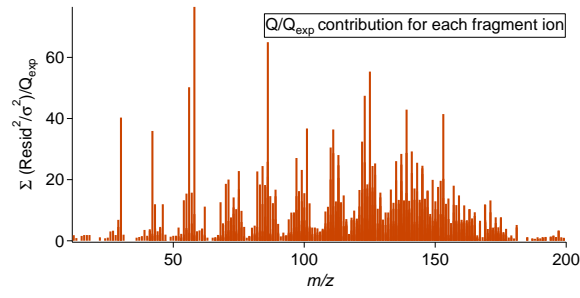
173



174



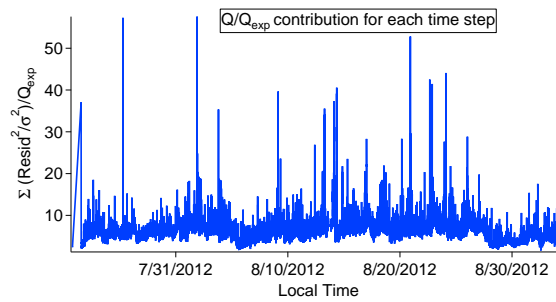
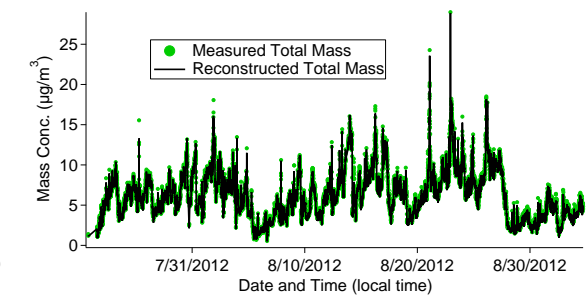
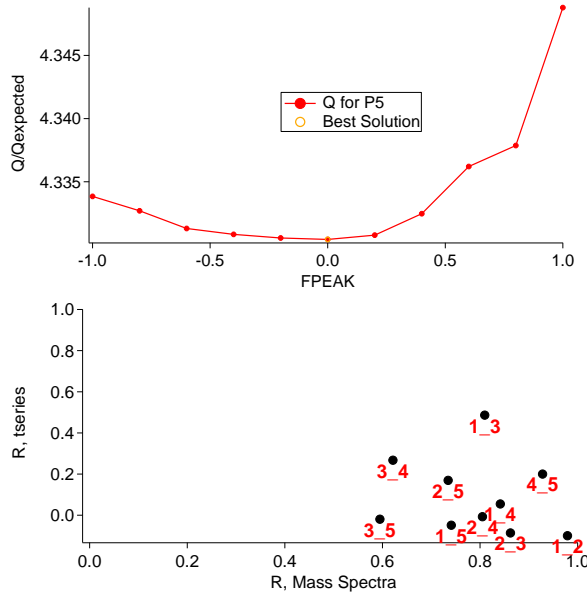
175



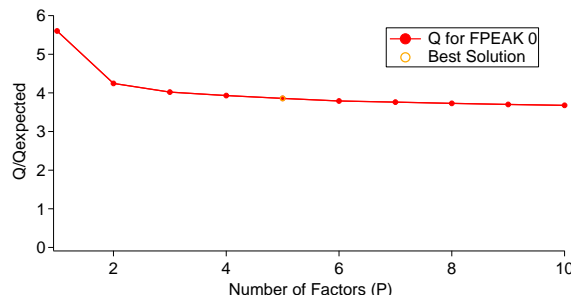
176

177

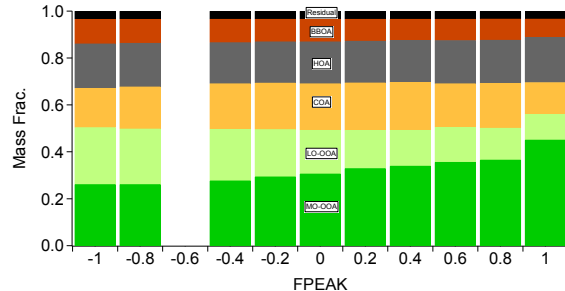
178



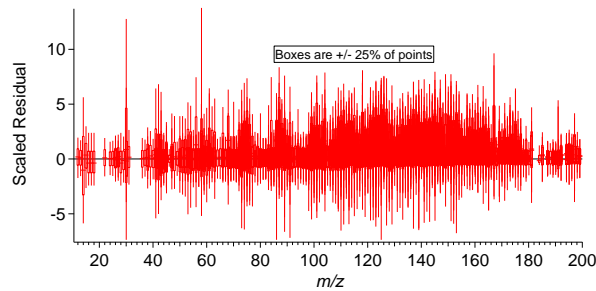
179 e) JST_Nov



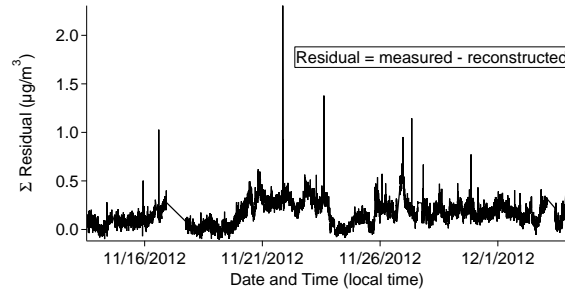
180



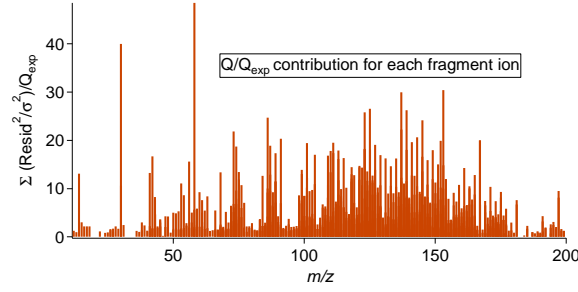
181



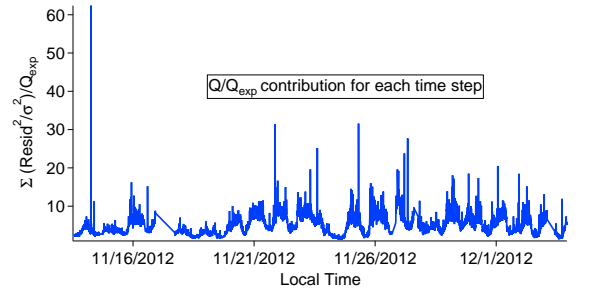
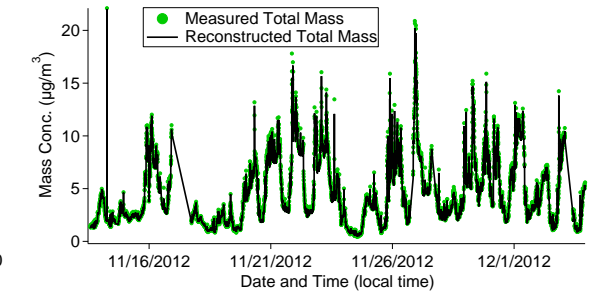
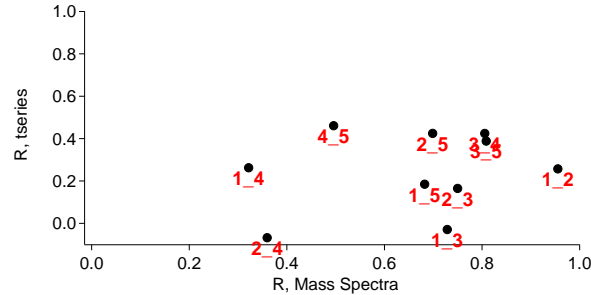
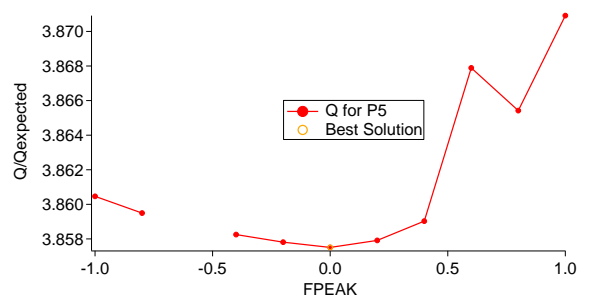
182



183



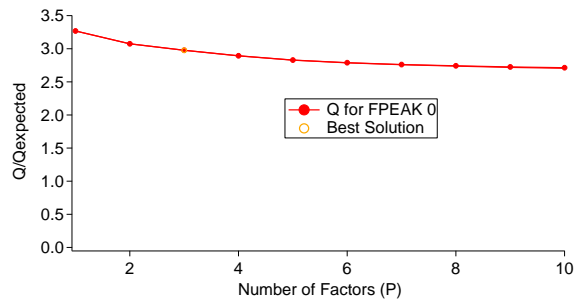
184



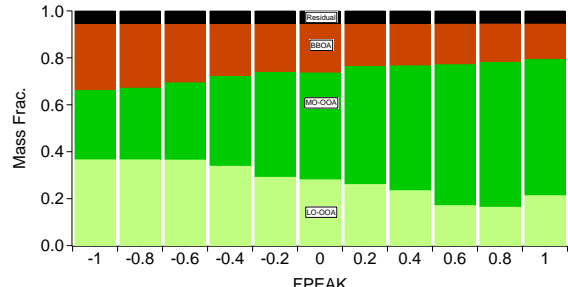
185

186

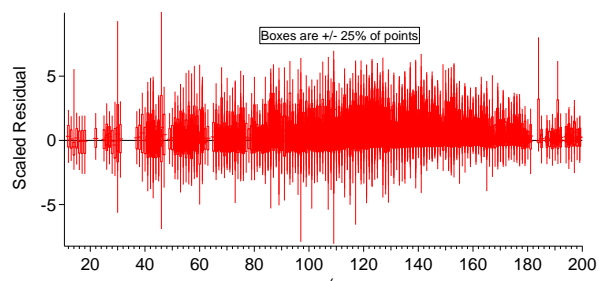
187 f) YRK_Dec



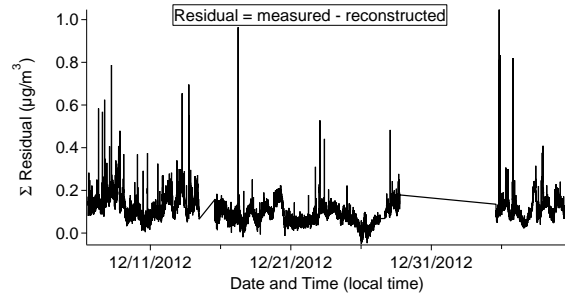
188



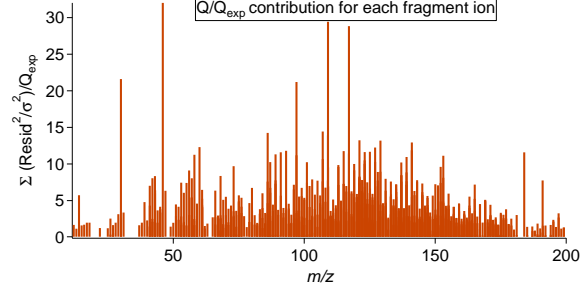
189



190



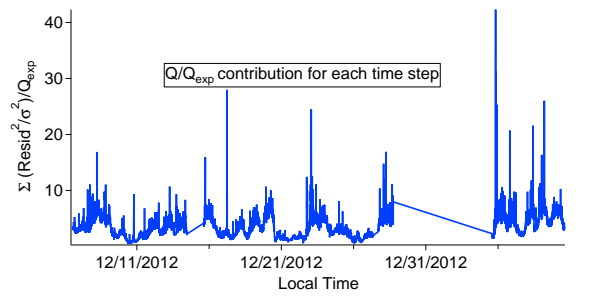
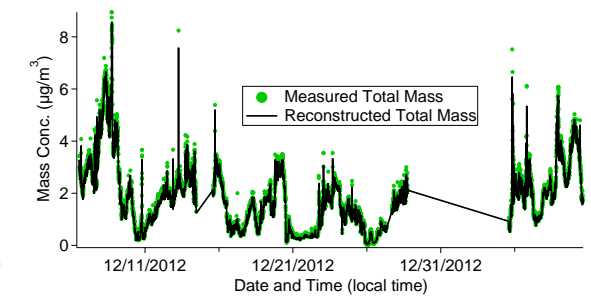
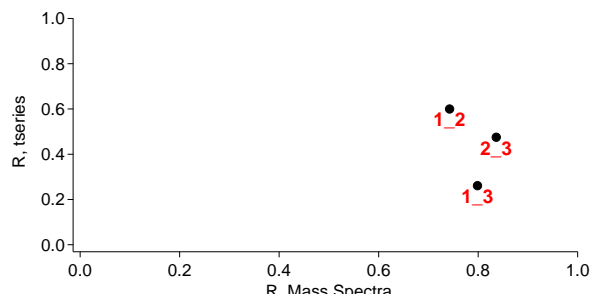
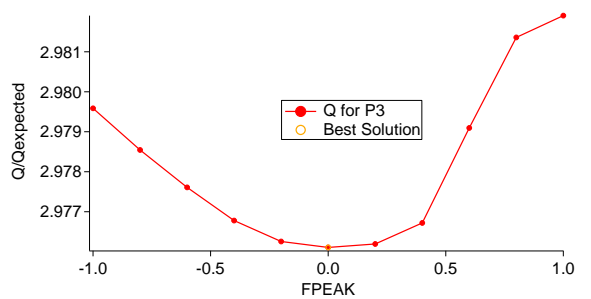
191



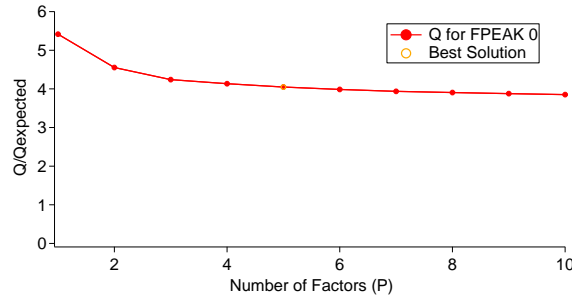
192

193

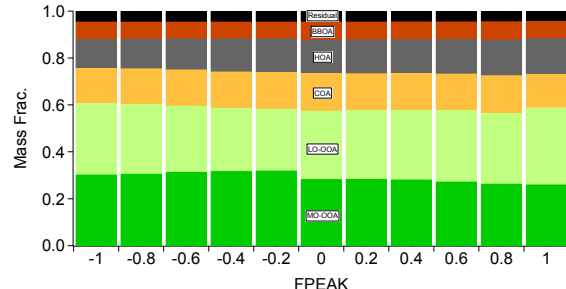
194



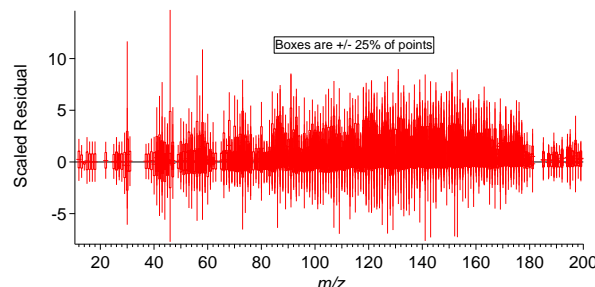
195 g) RS_Jan



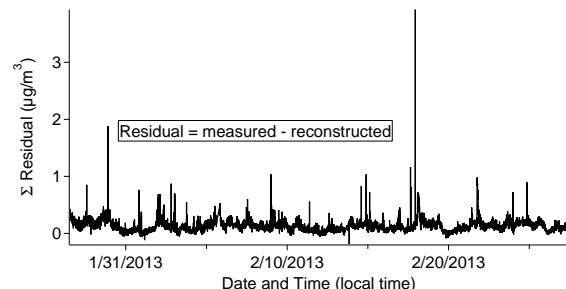
196



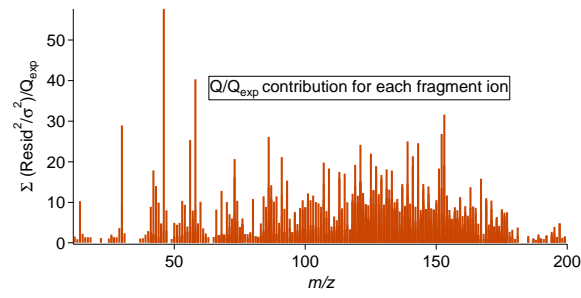
197



198



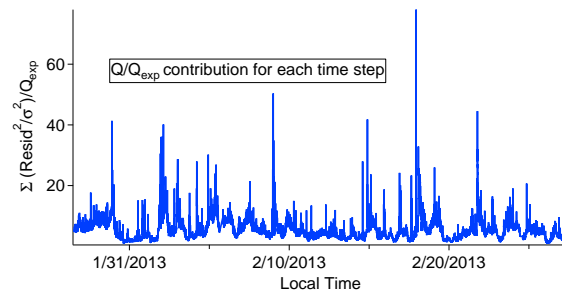
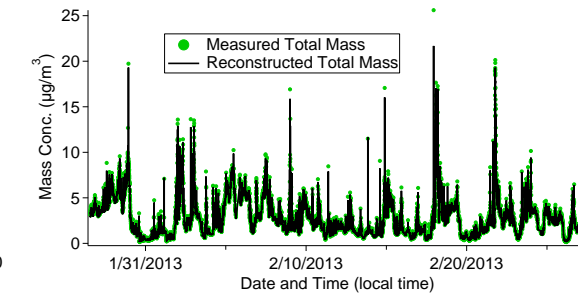
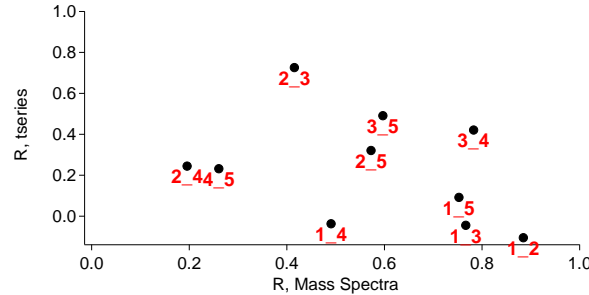
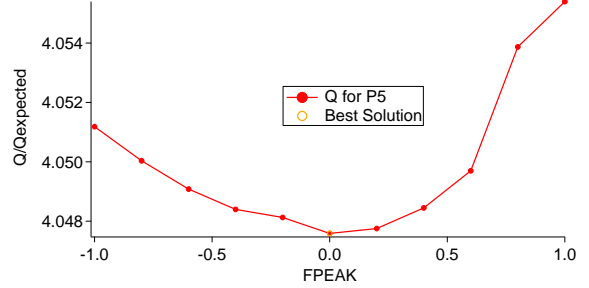
199



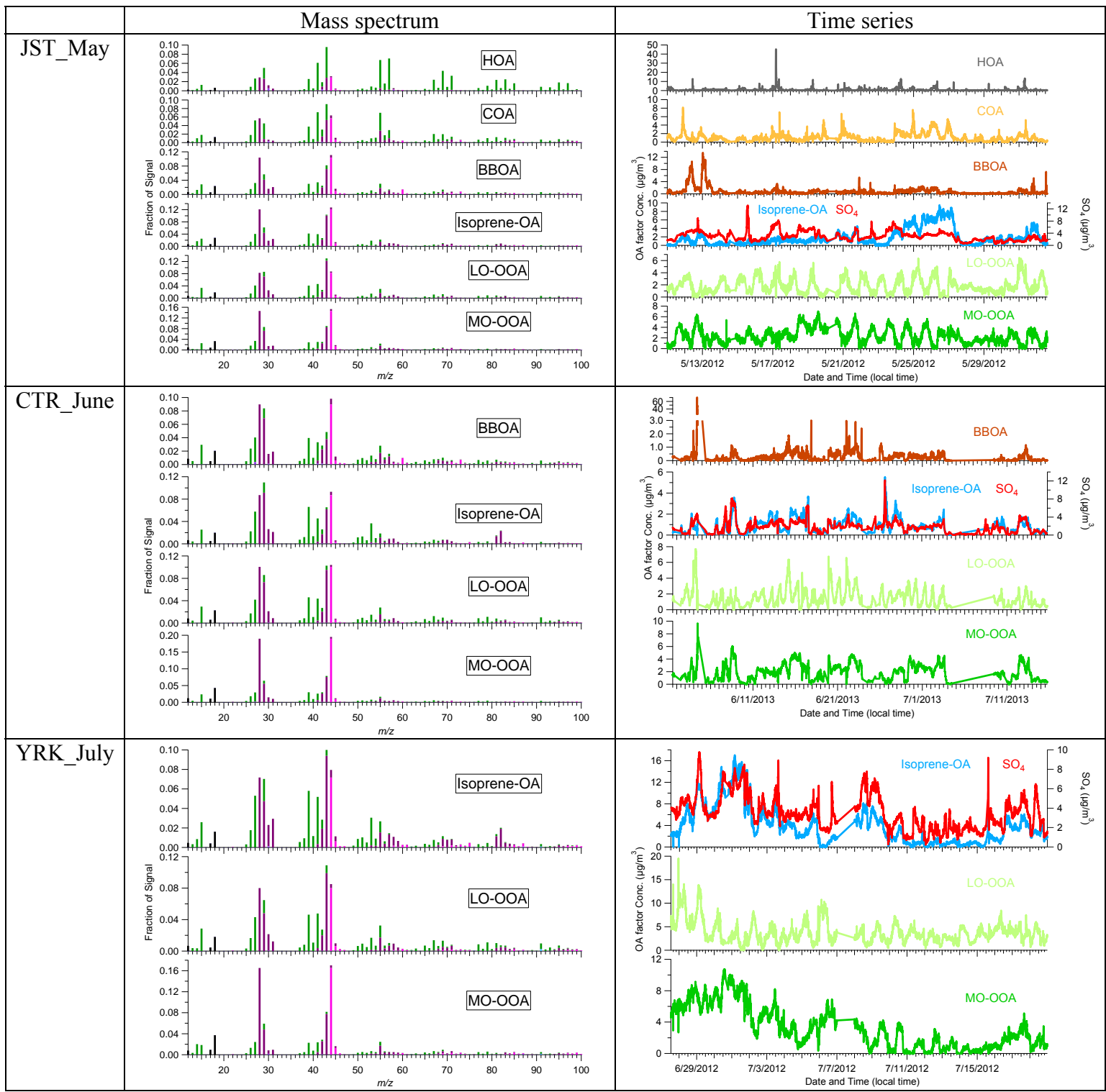
200

201

202



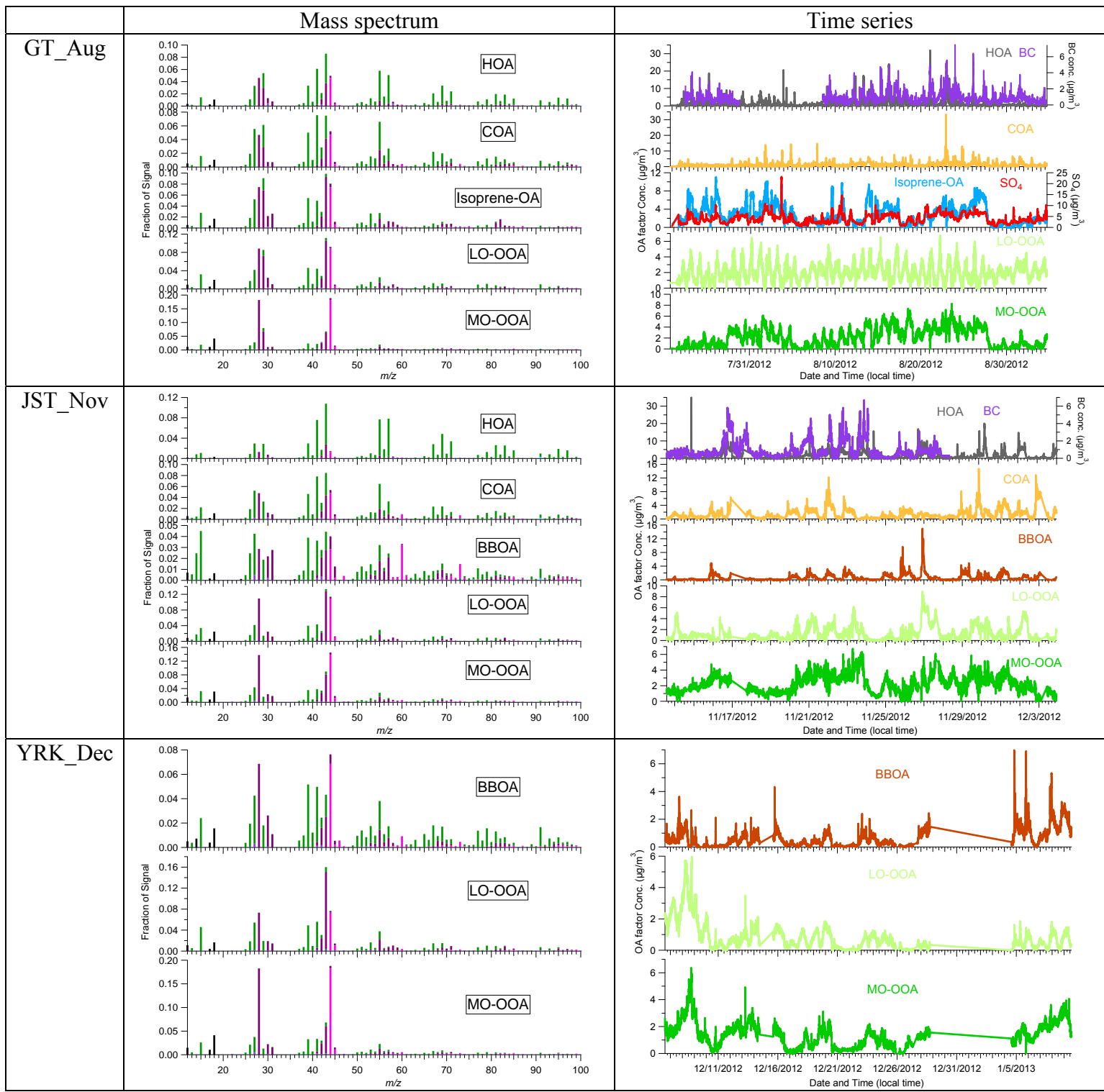
203 Fig. S2.



204

205

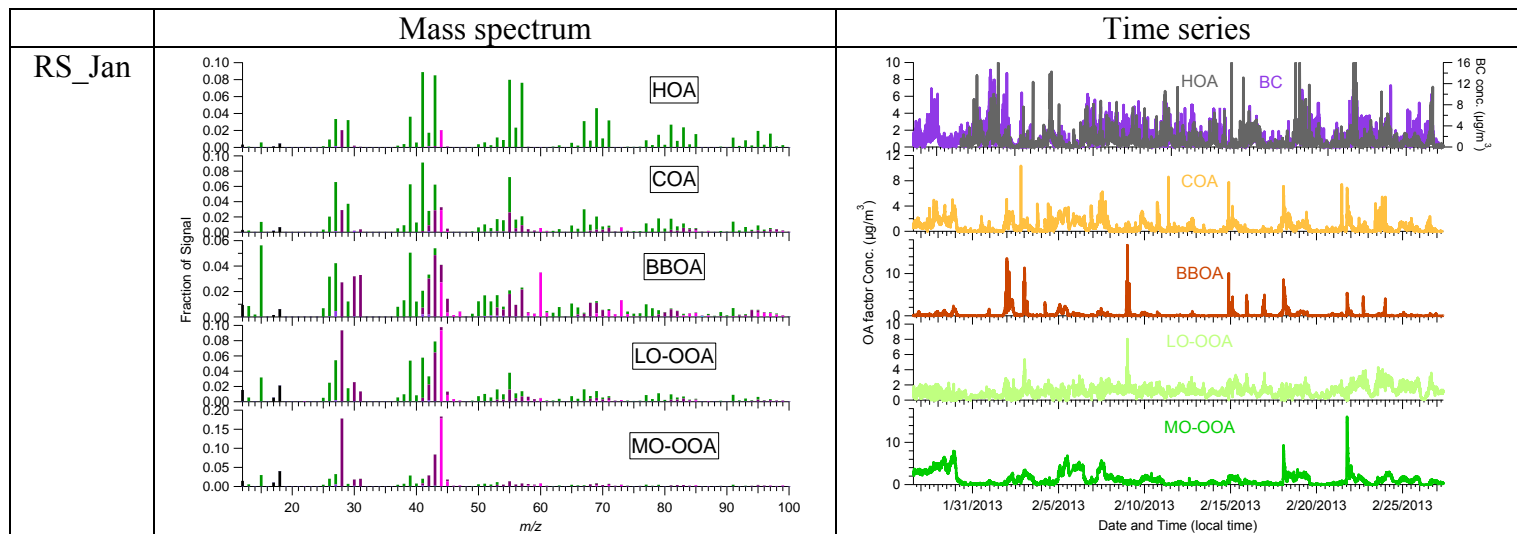
206 Fig. S2. Continued



207

208

209 Fig. S2. Continued



210

211

212

213

214

215

216

217

218

219

220

221

222

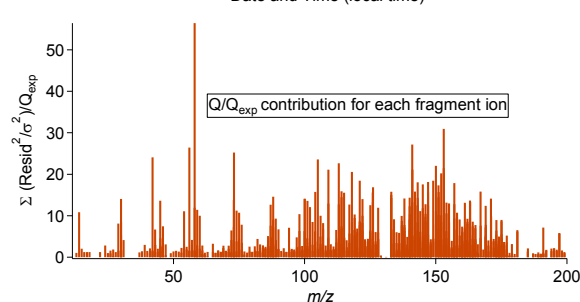
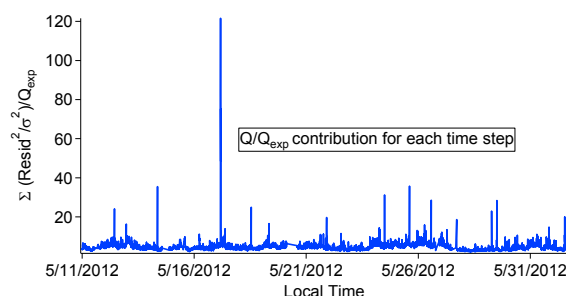
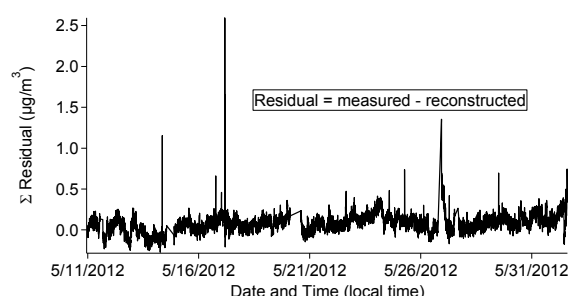
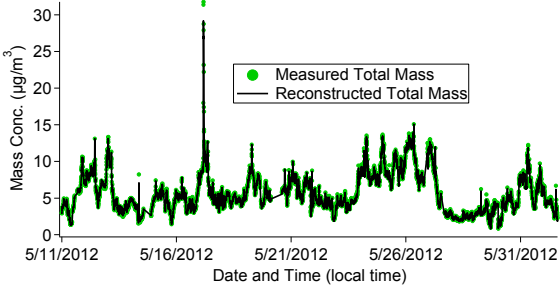
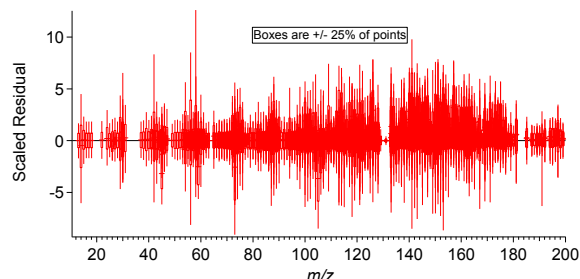
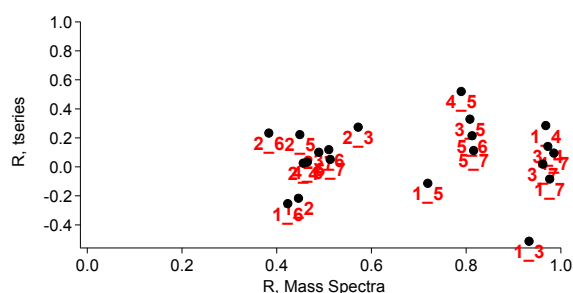
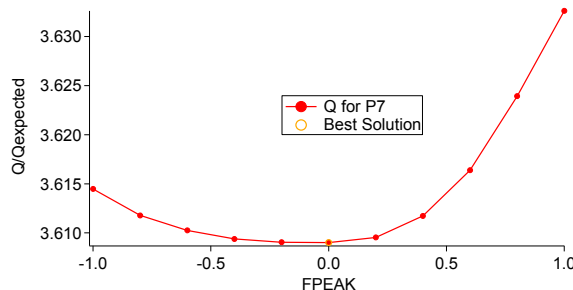
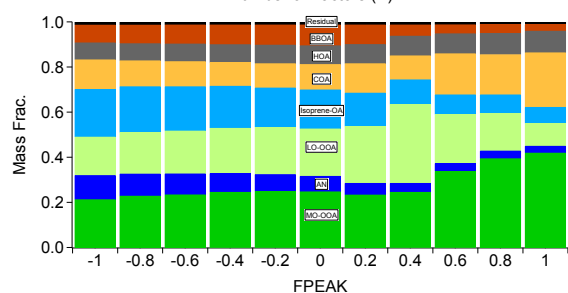
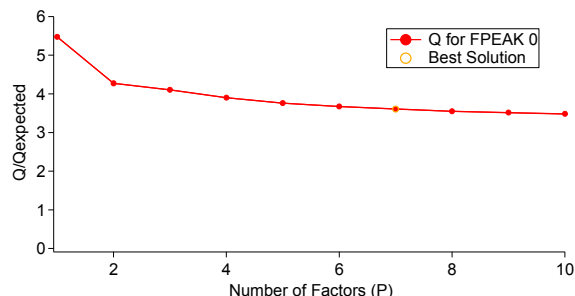
223

224

225

226 Fig. S3.

227 (a) JST_May



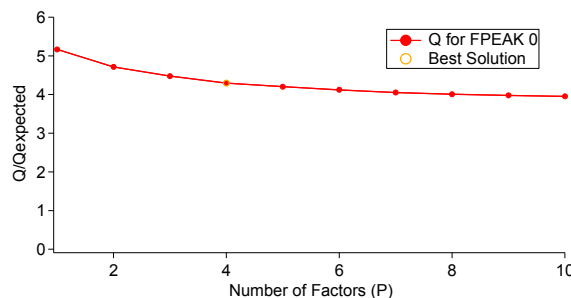
232

233

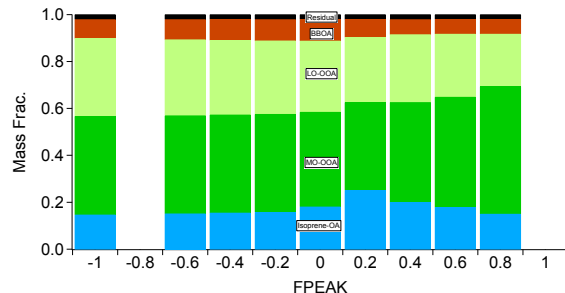
234

235

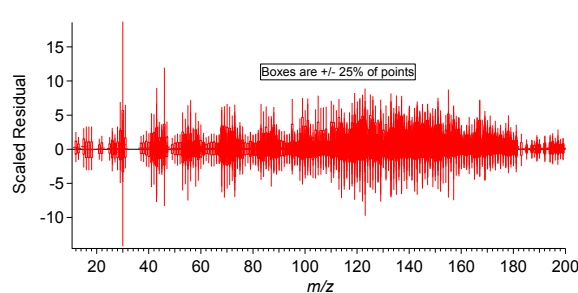
236 (b) CTR_June



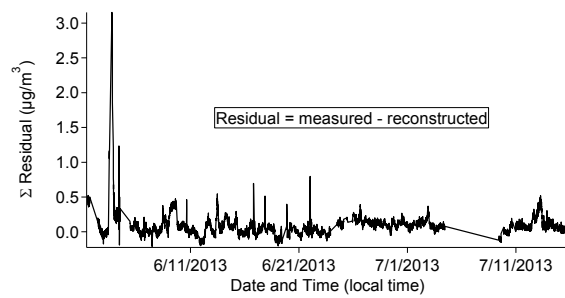
237



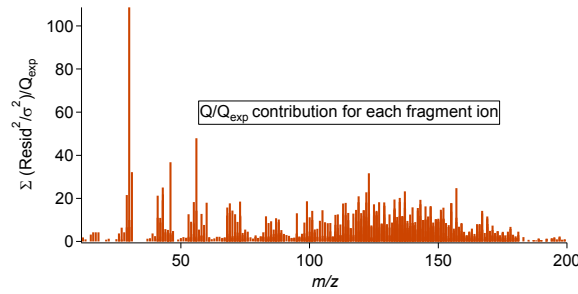
238



239



240



241

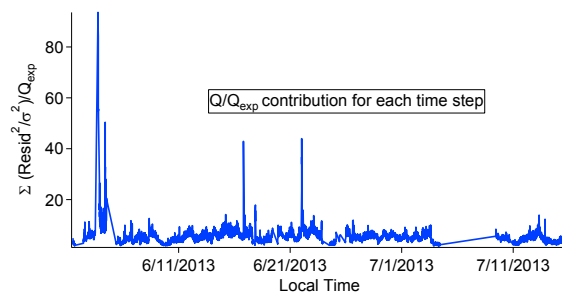
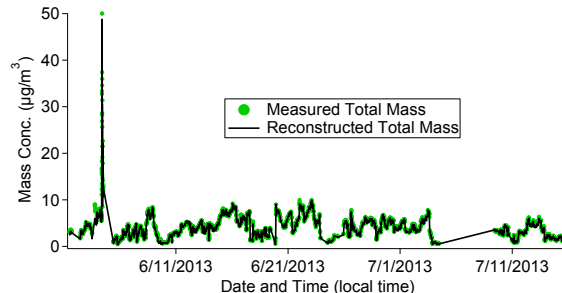
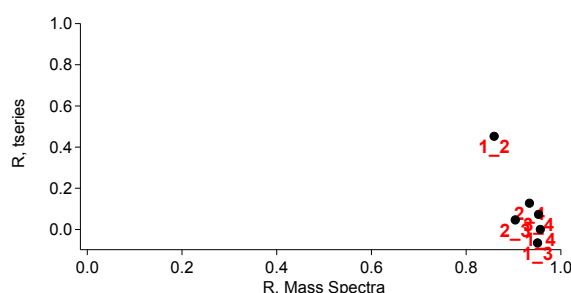
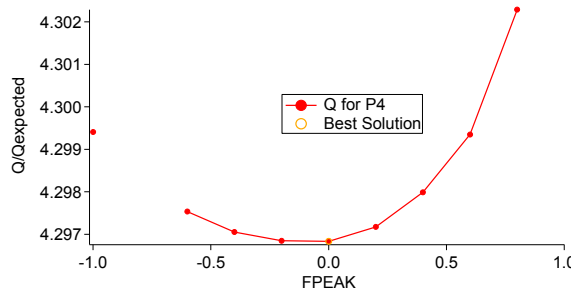
242

243

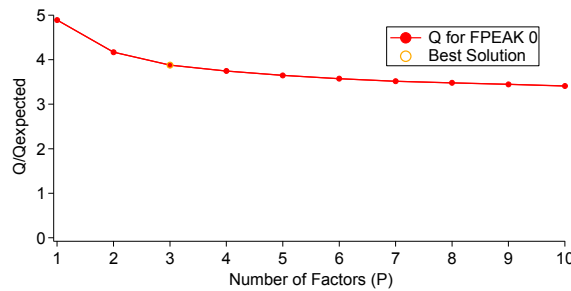
244

245

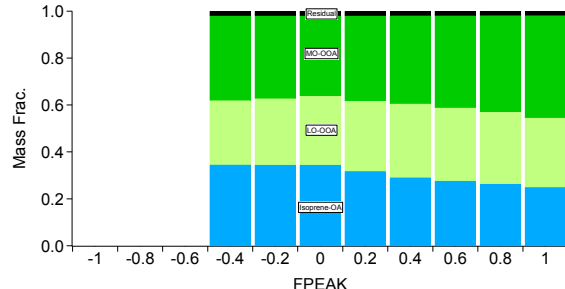
246



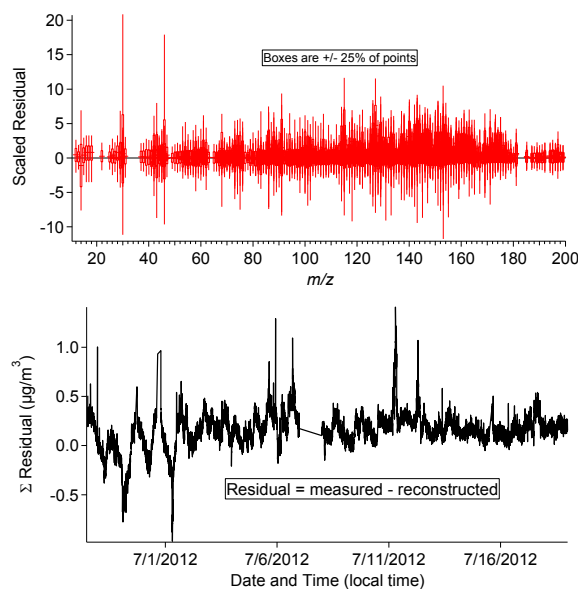
247 (c) YRK_July



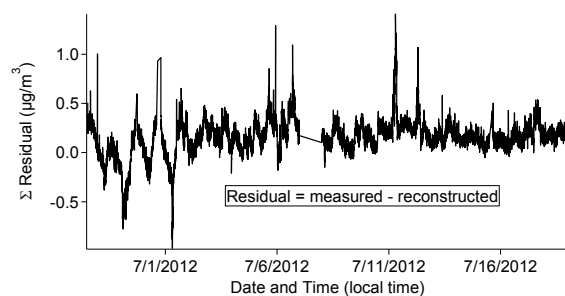
248



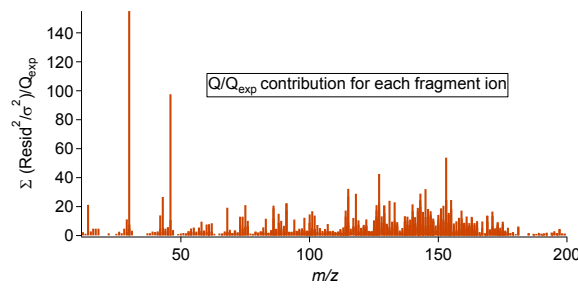
249



250



251



252

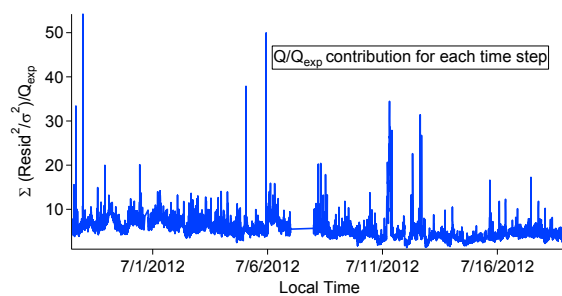
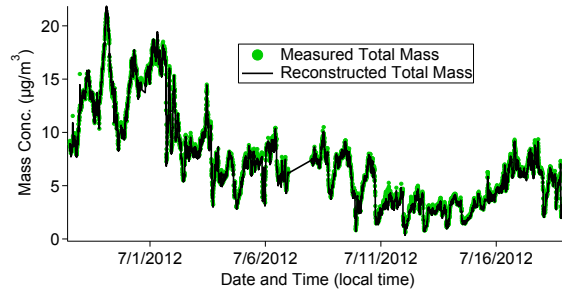
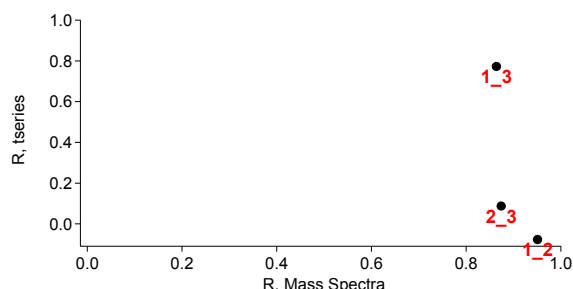
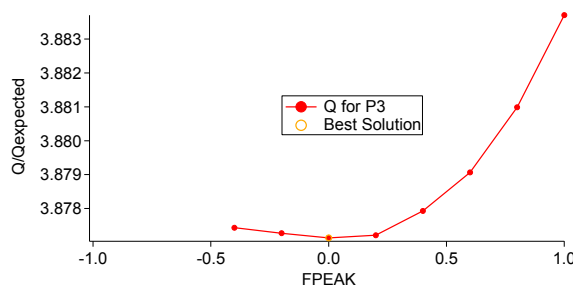
253

254

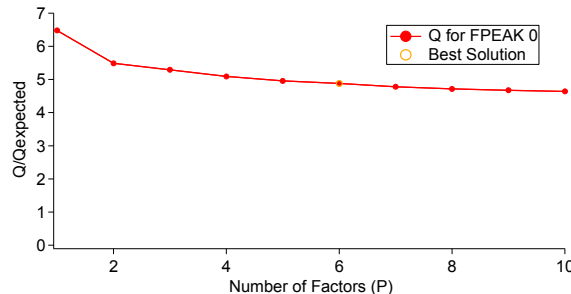
255

256

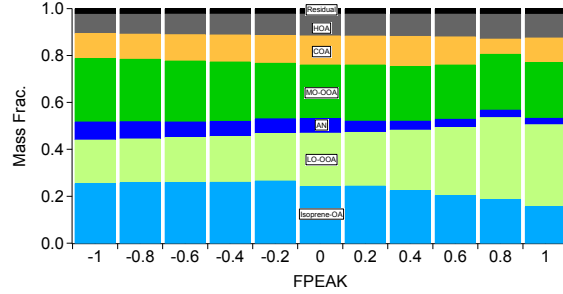
257



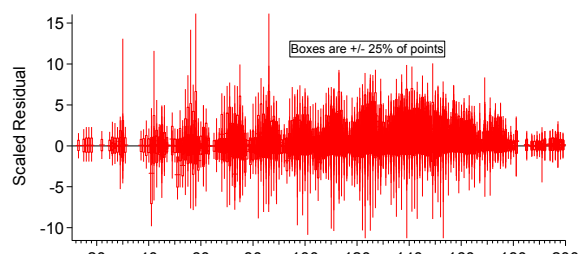
258 (d) GT_Aug



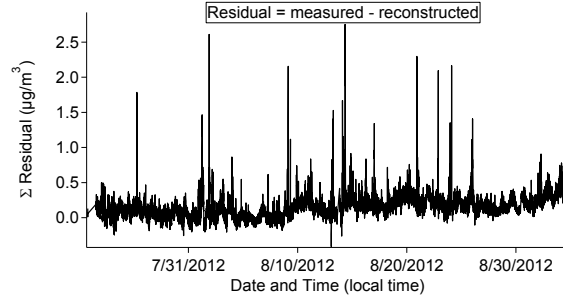
259



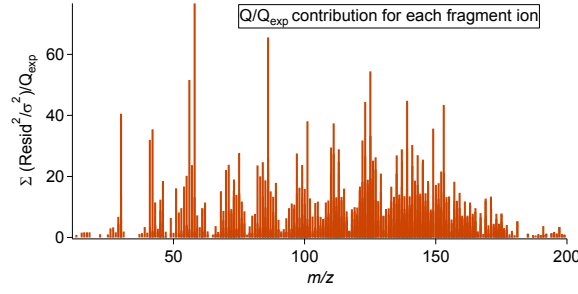
260



261



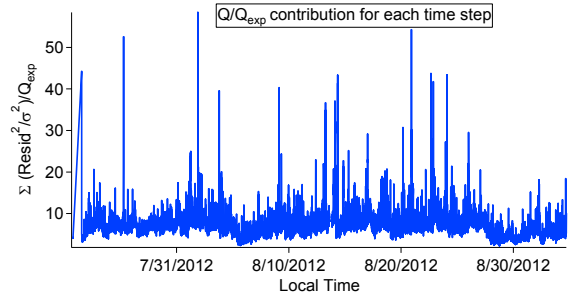
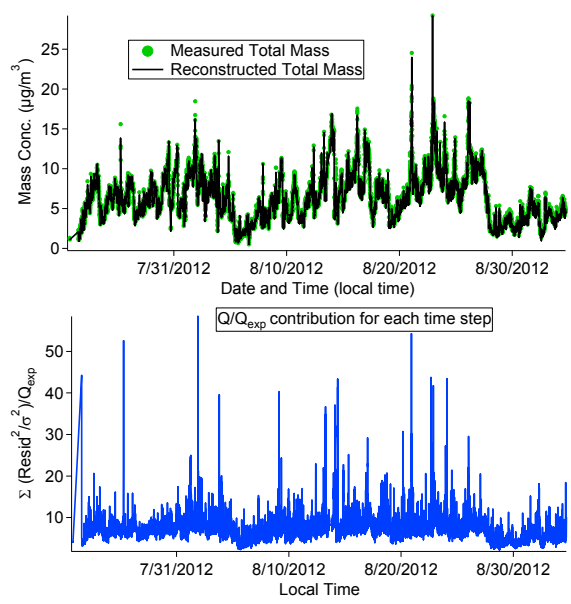
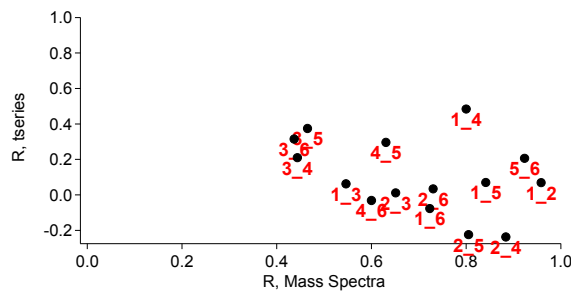
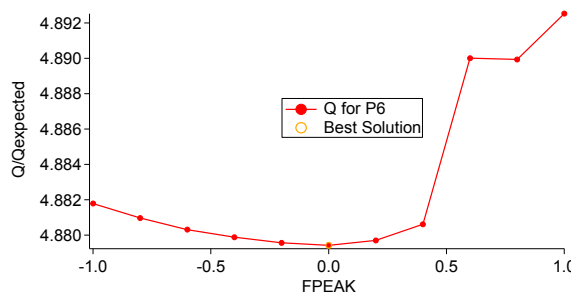
262



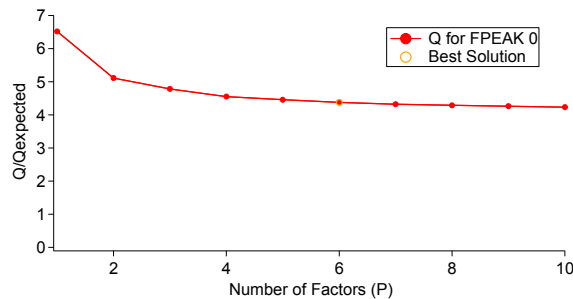
263

264

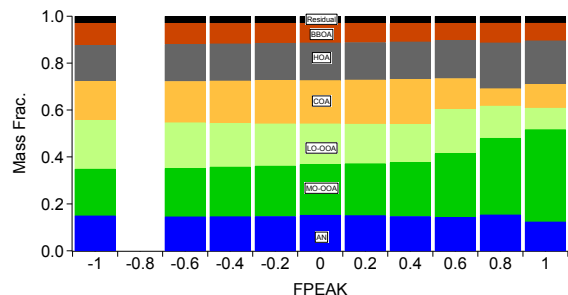
265



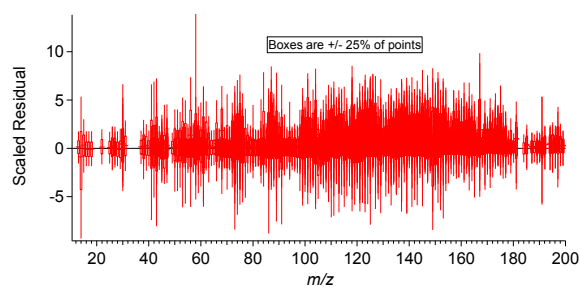
266 (e) JST_Nov



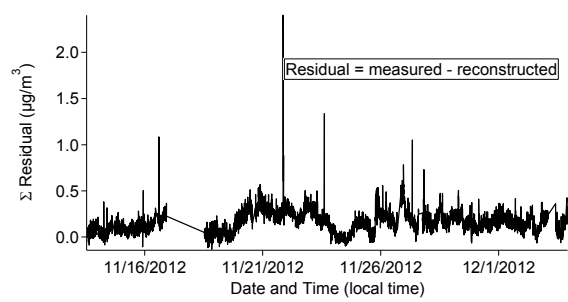
267



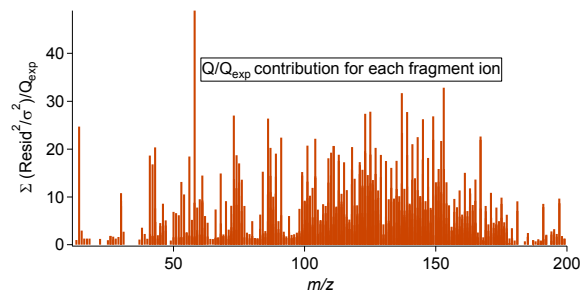
268



269



270

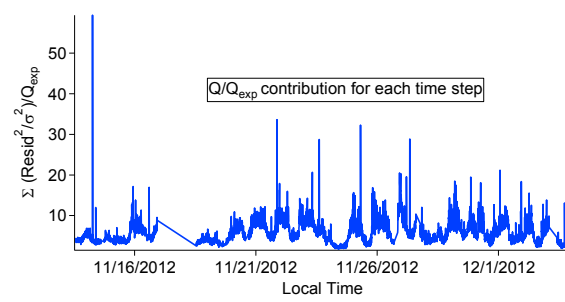
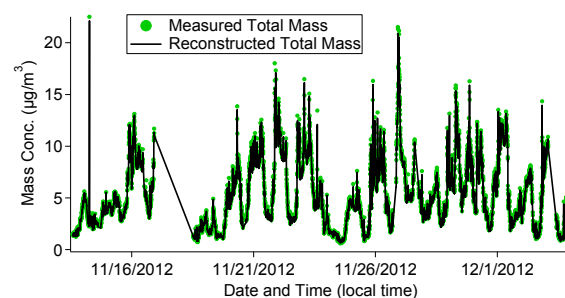
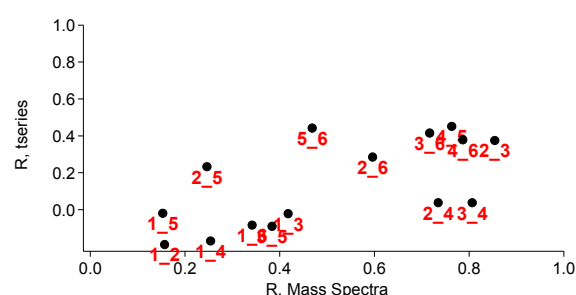
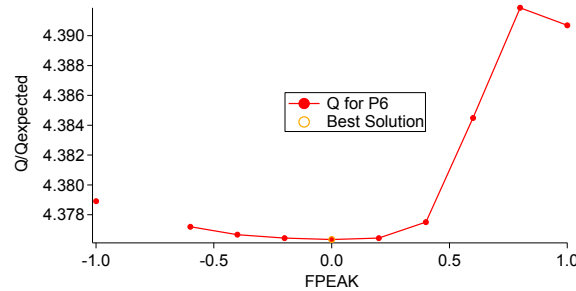


271

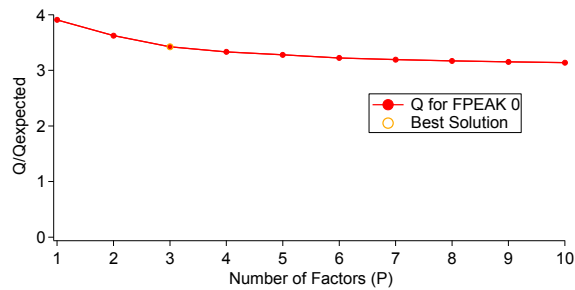
272

273

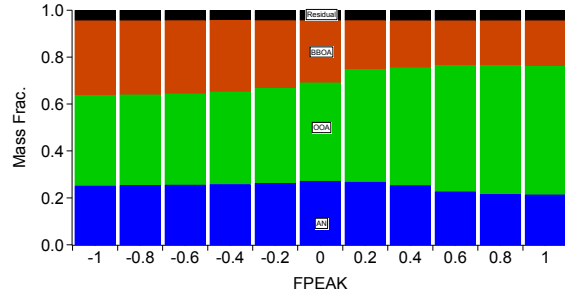
274



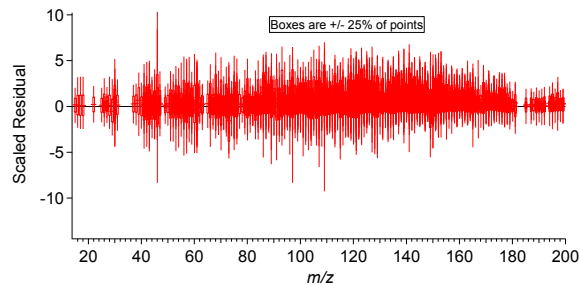
275 (f) YRK_Dec



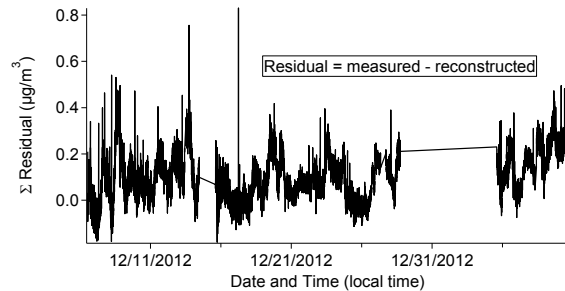
276



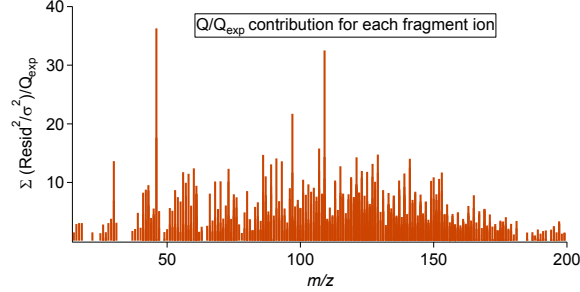
277



278



279

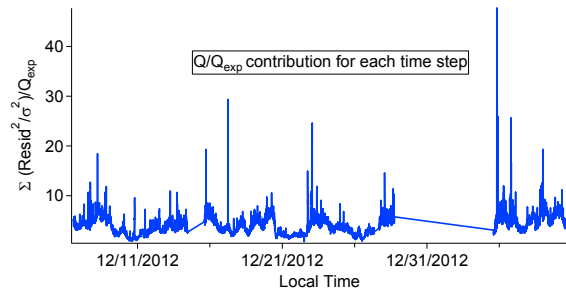
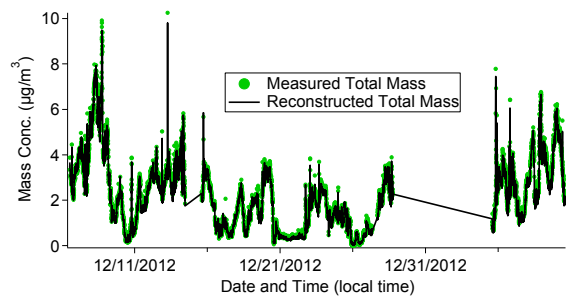
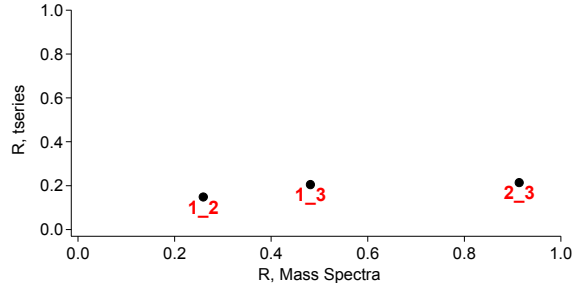
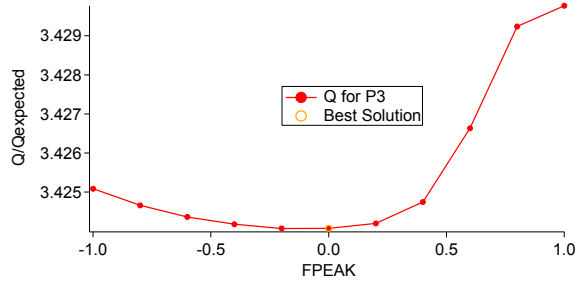


280

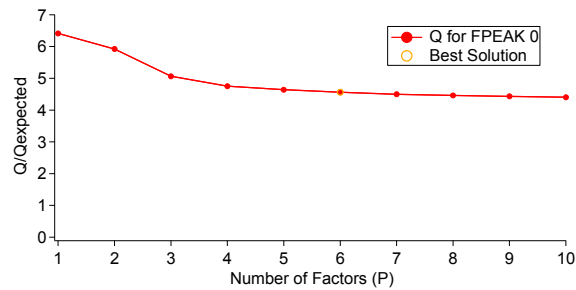
281

282

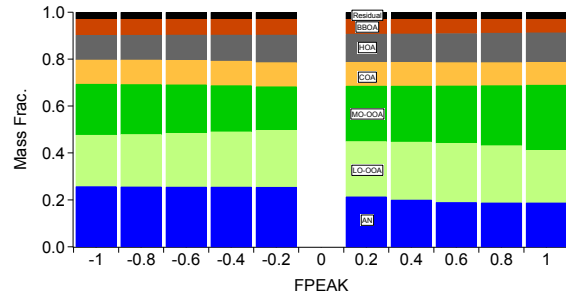
283



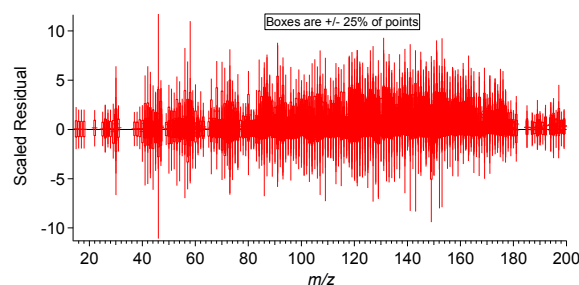
284 (g) RS_Jan



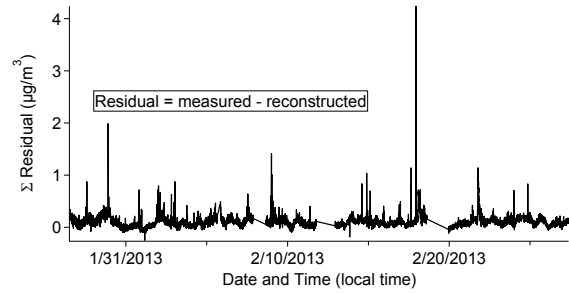
285



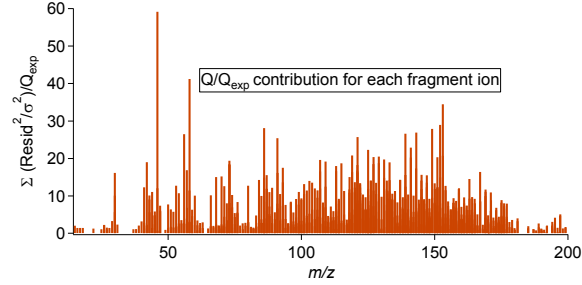
286



287



288



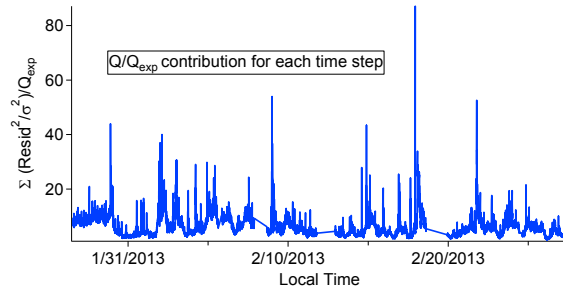
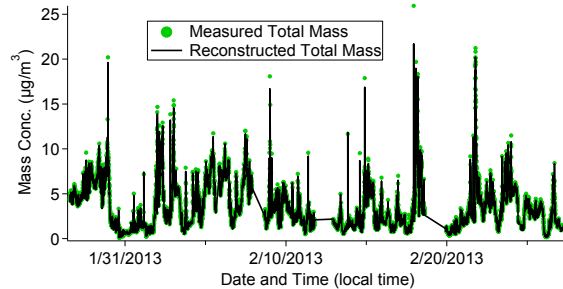
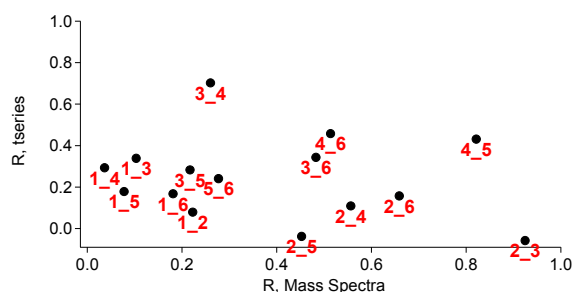
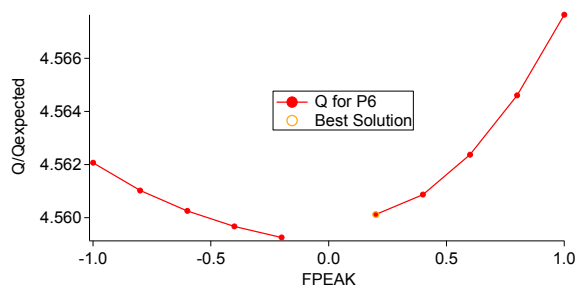
289

290

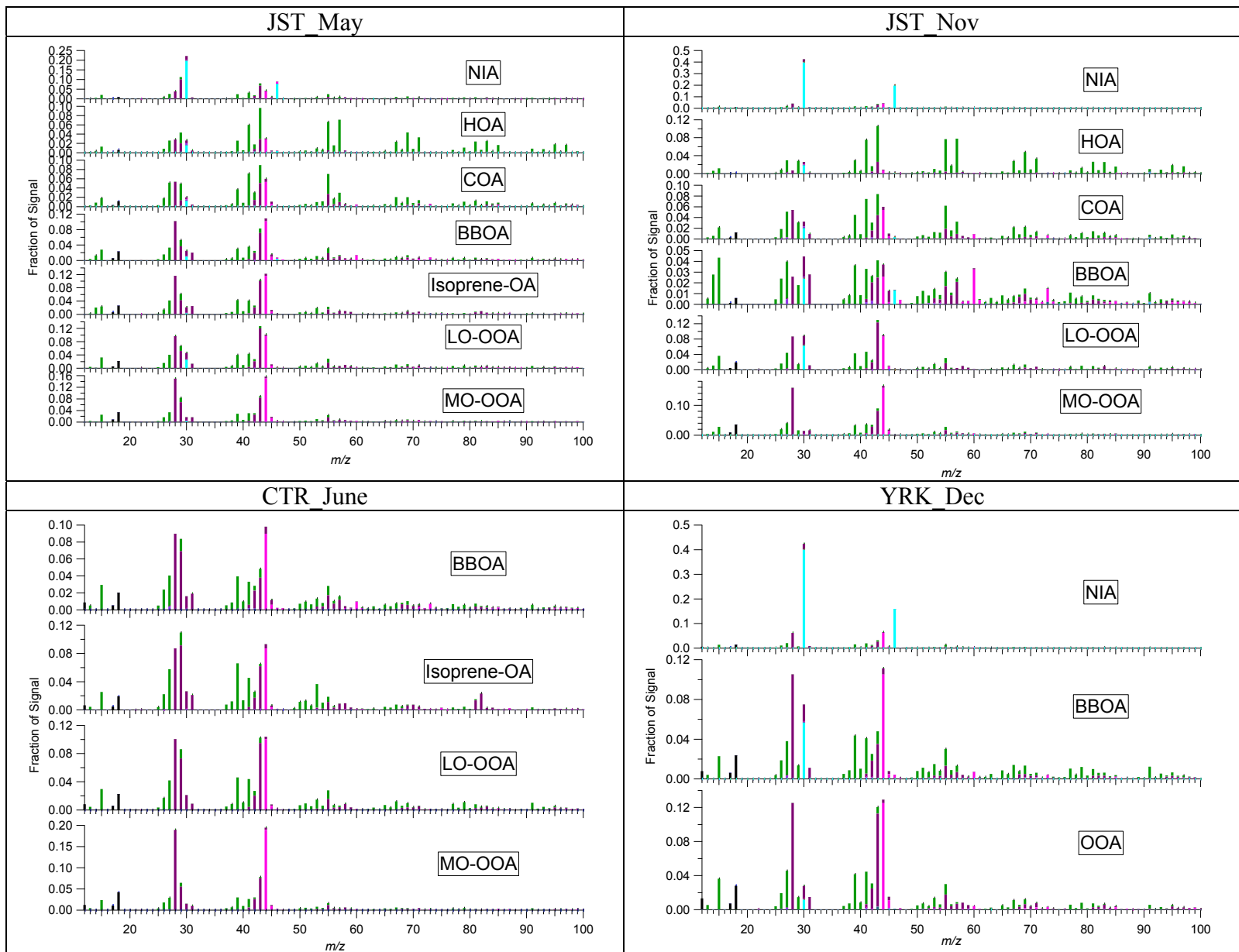
291

292

293



294 Fig. S4.



295

296

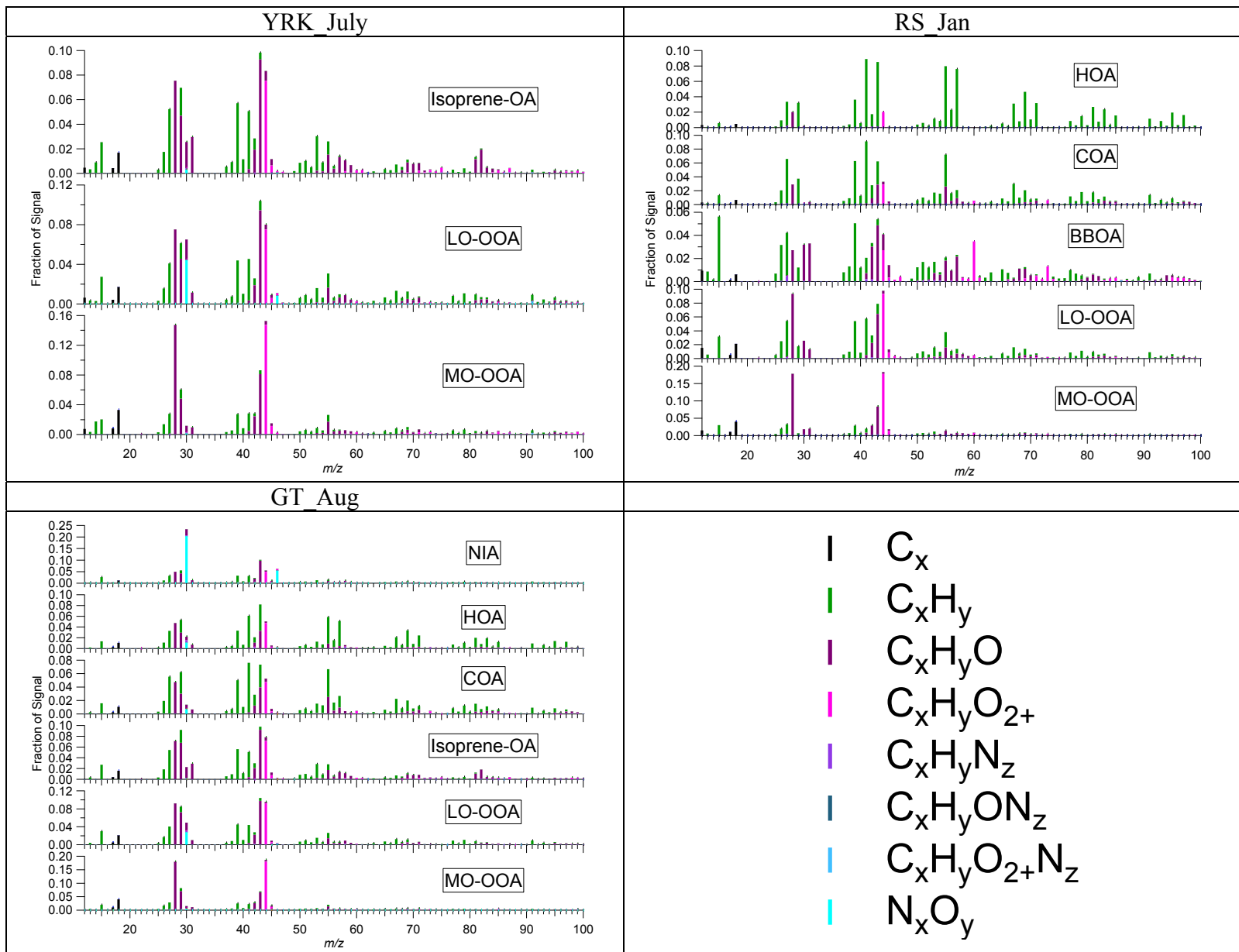
297

298

299

300

301 Fig. S4 continued



302

303

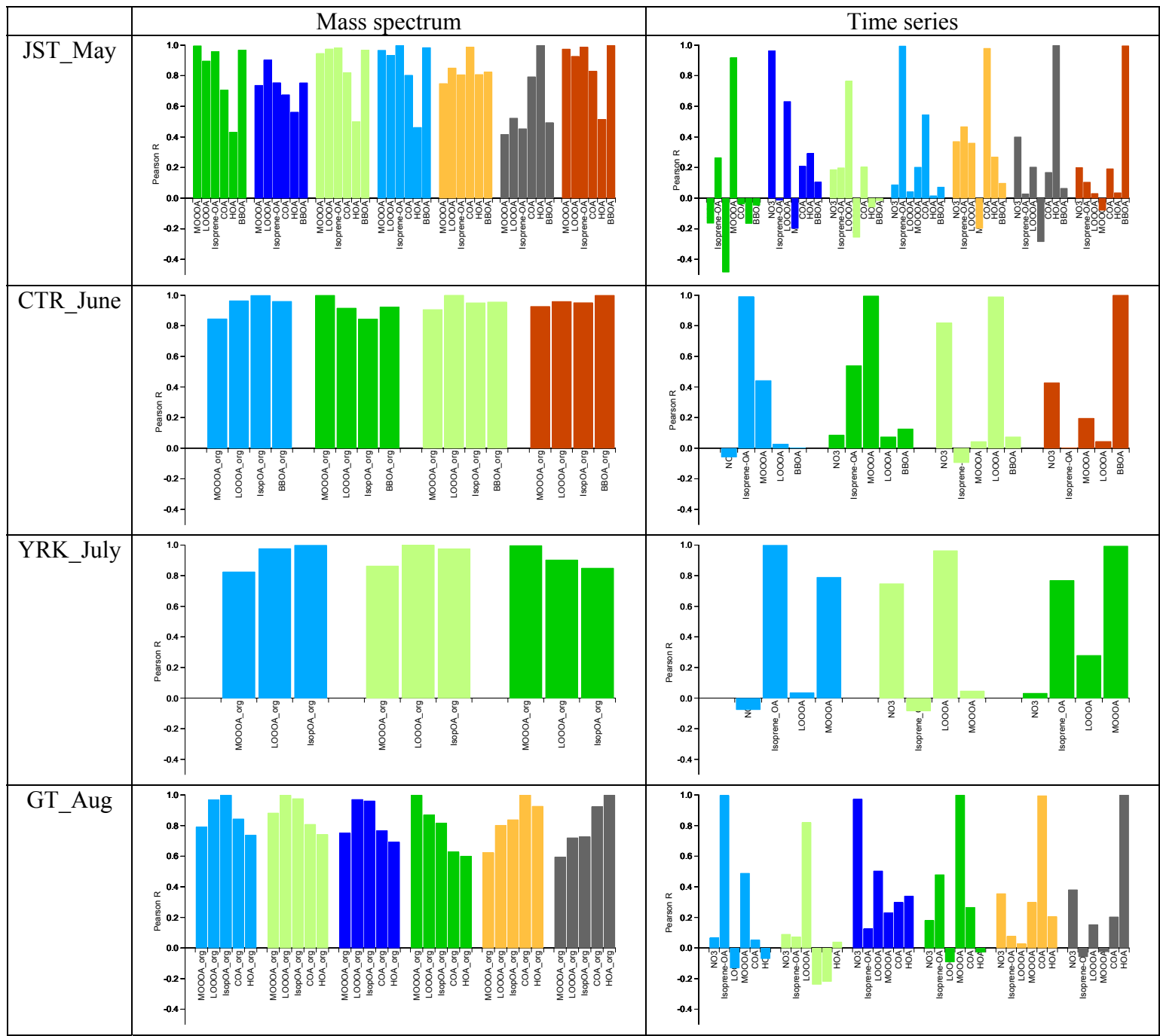
304

305

306

307

308 Fig. S5.



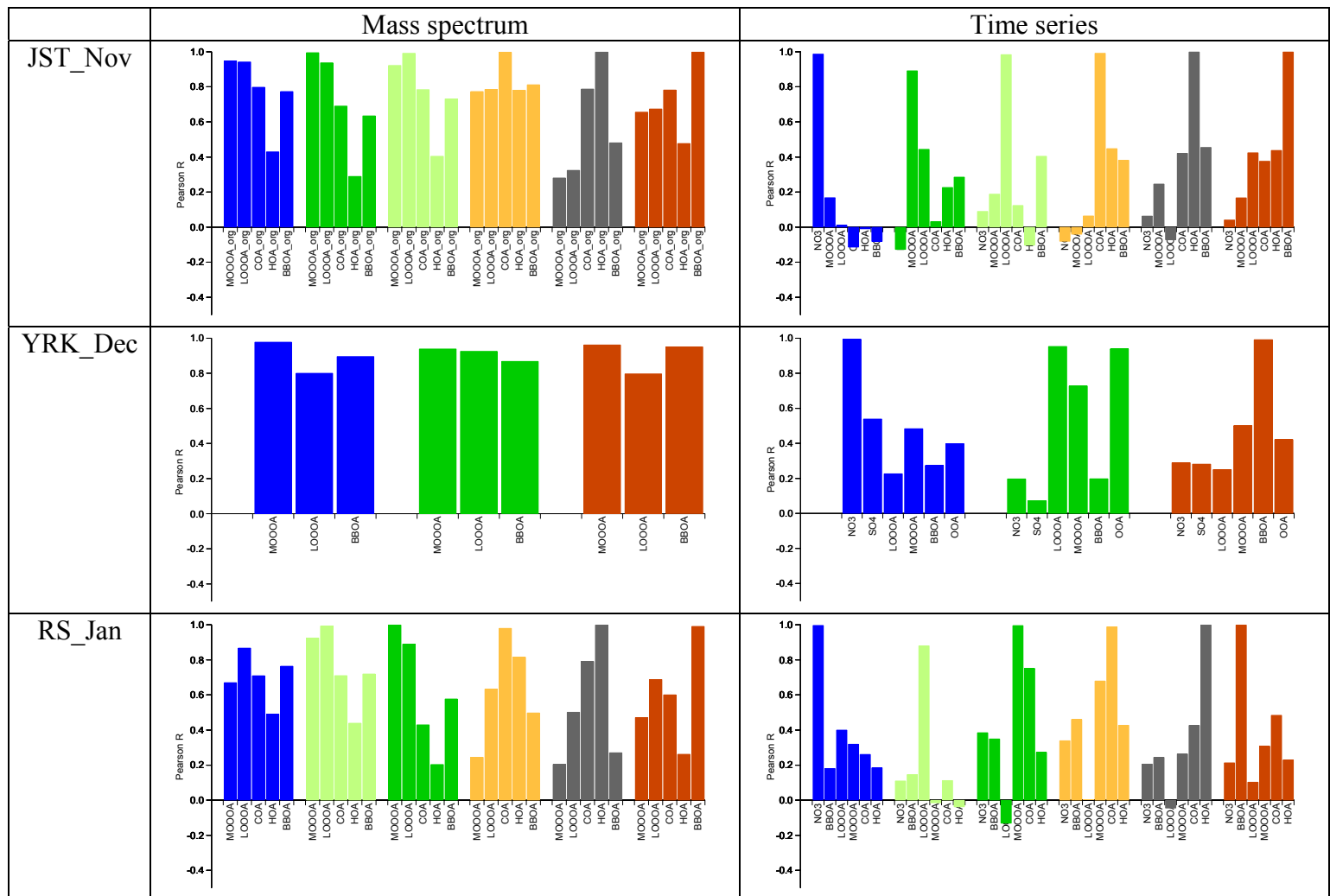
309

310

311

312

313 Fig. S5. Continued



314

315

316

317

318

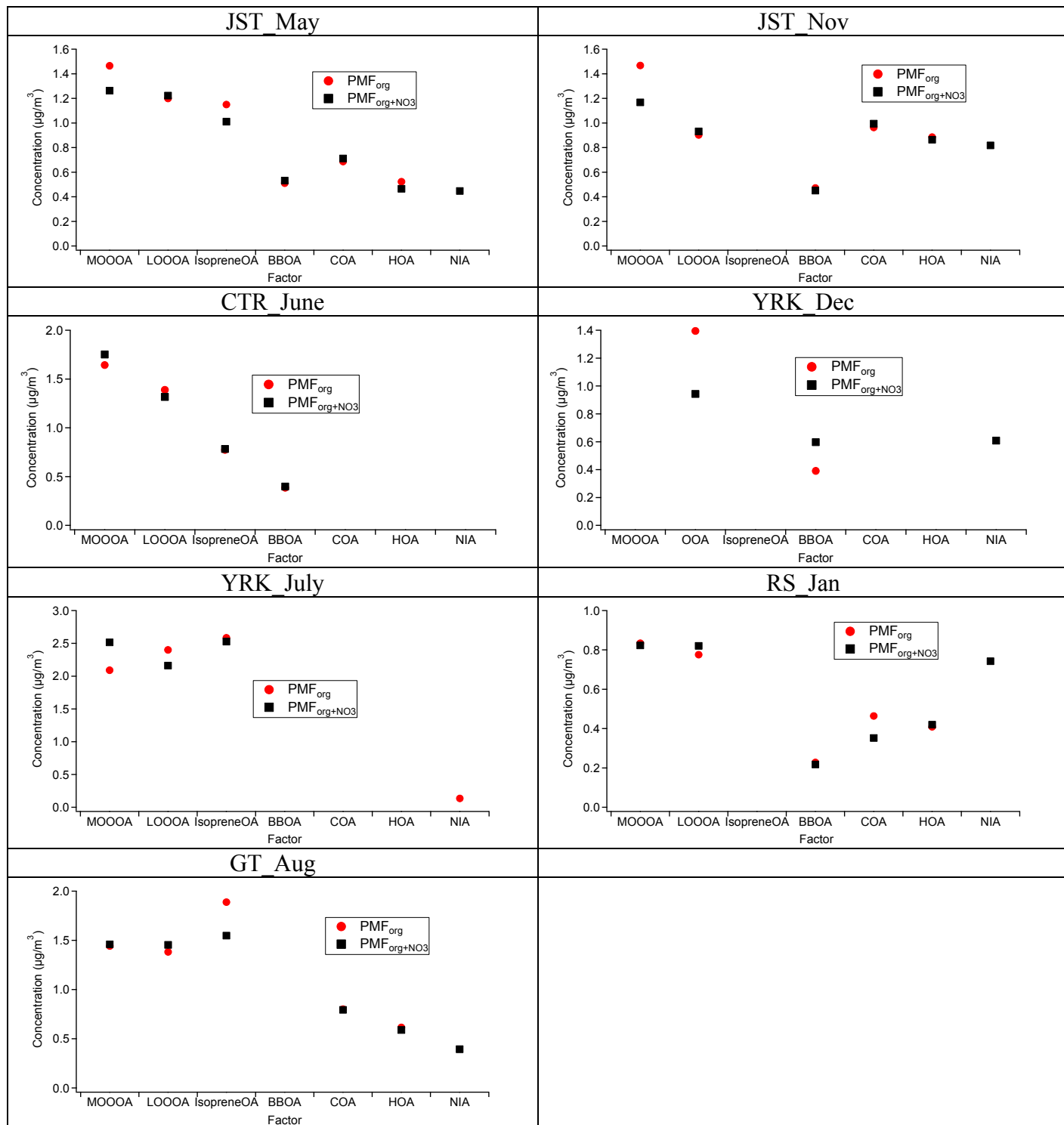
319

320

321

322

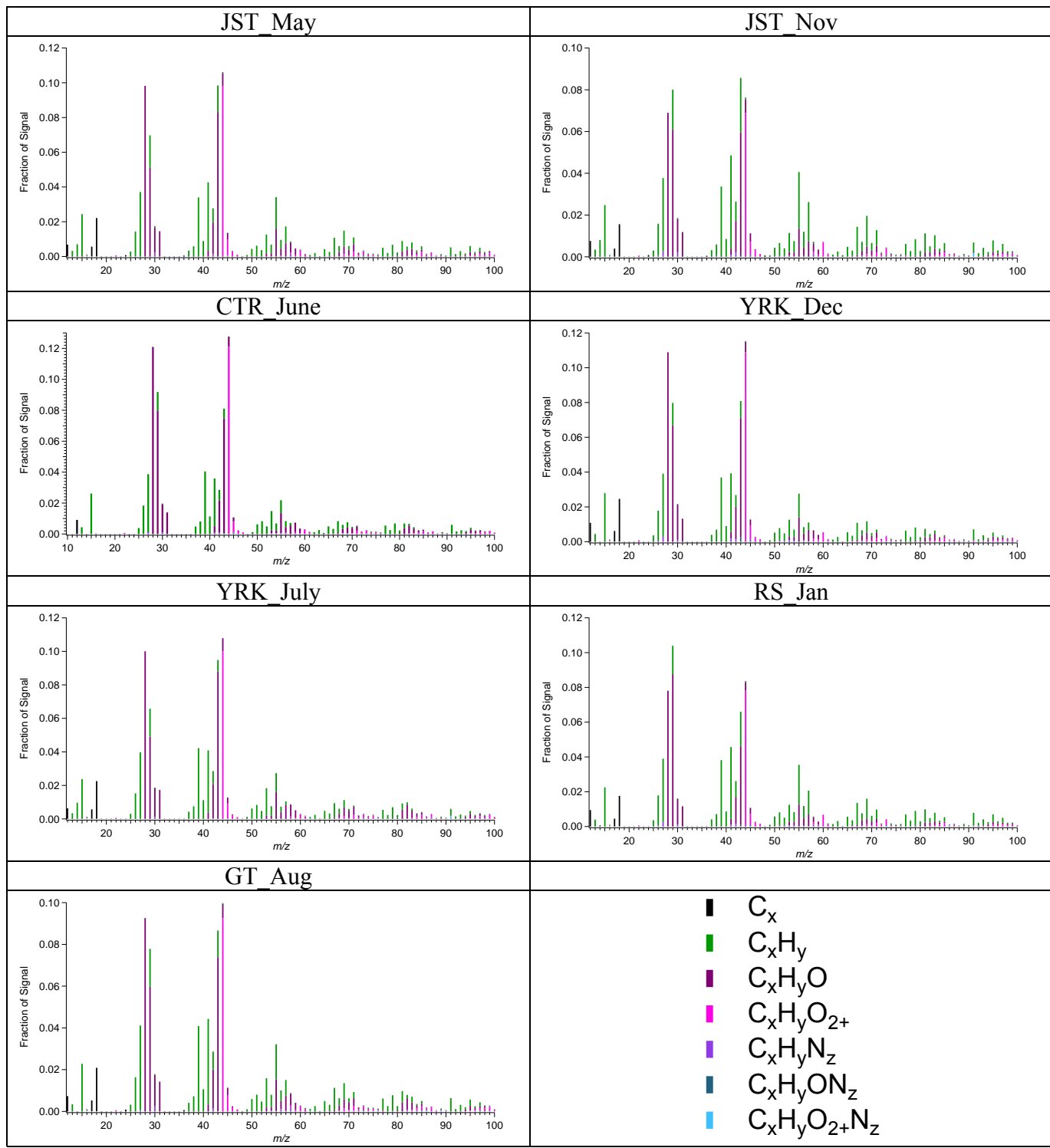
323 Fig. S6.



324

325

326 Fig. S7.

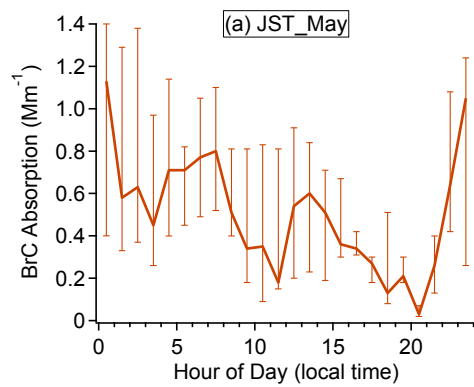


327

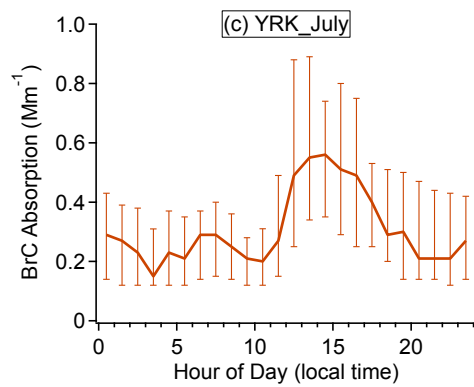
328

329 Fig. S8.

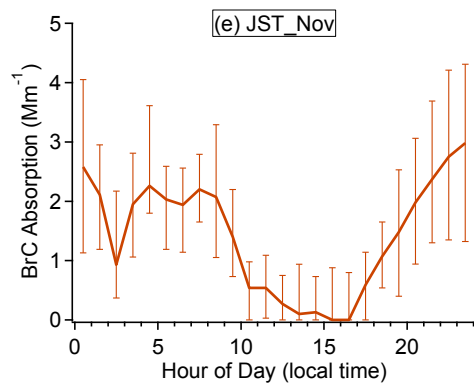
330



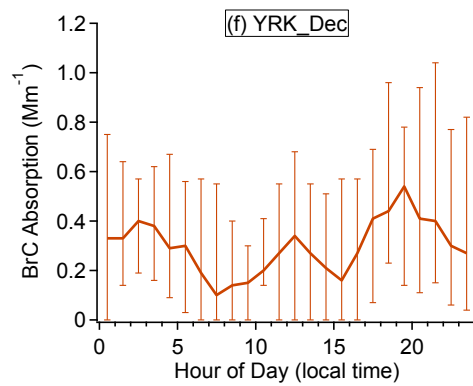
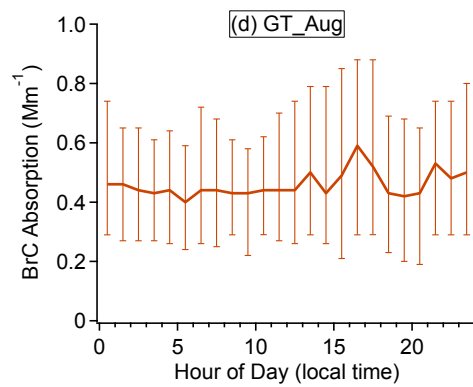
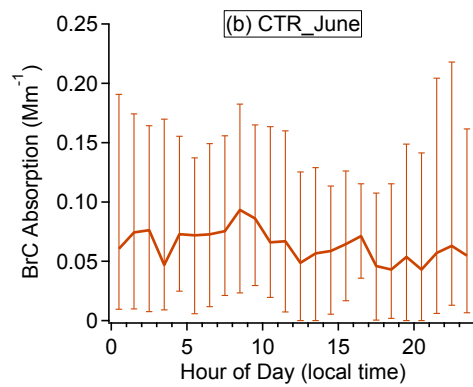
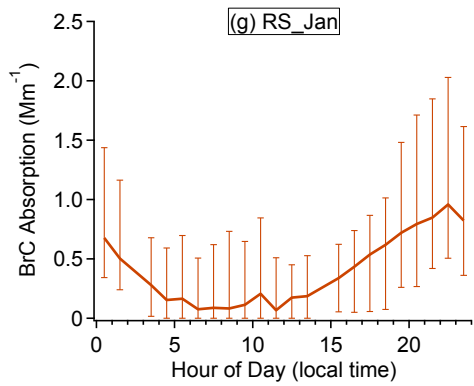
331



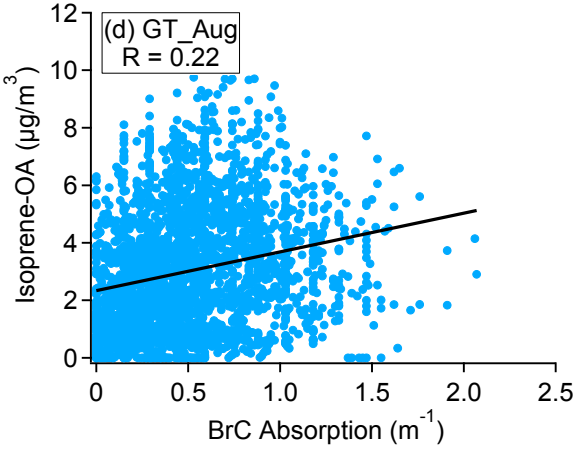
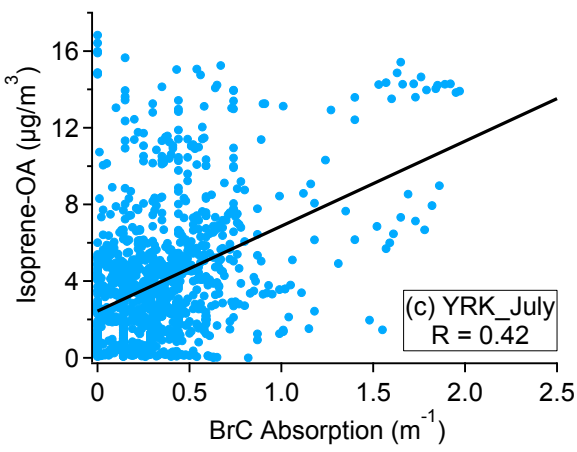
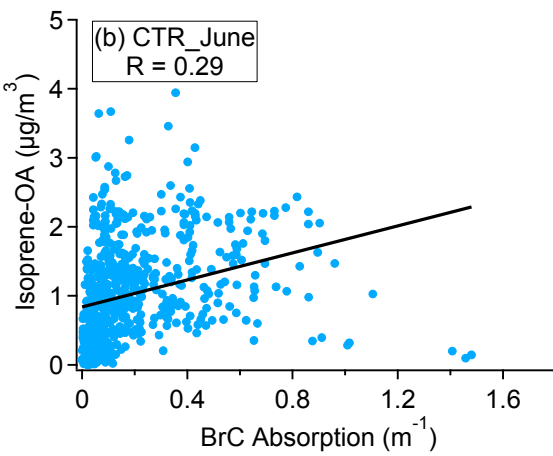
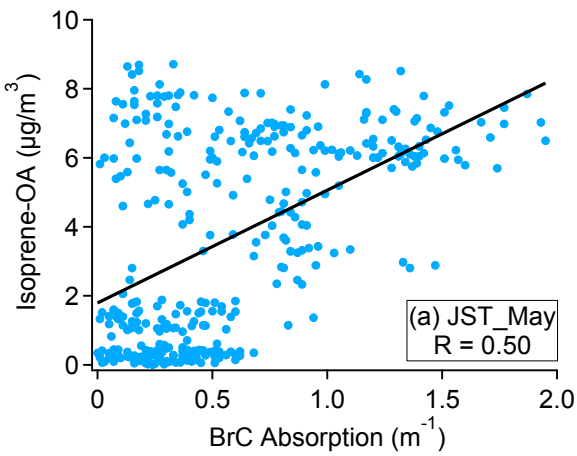
332



333



334 Fig. S9.



335

336

337

338

339

340

341

342

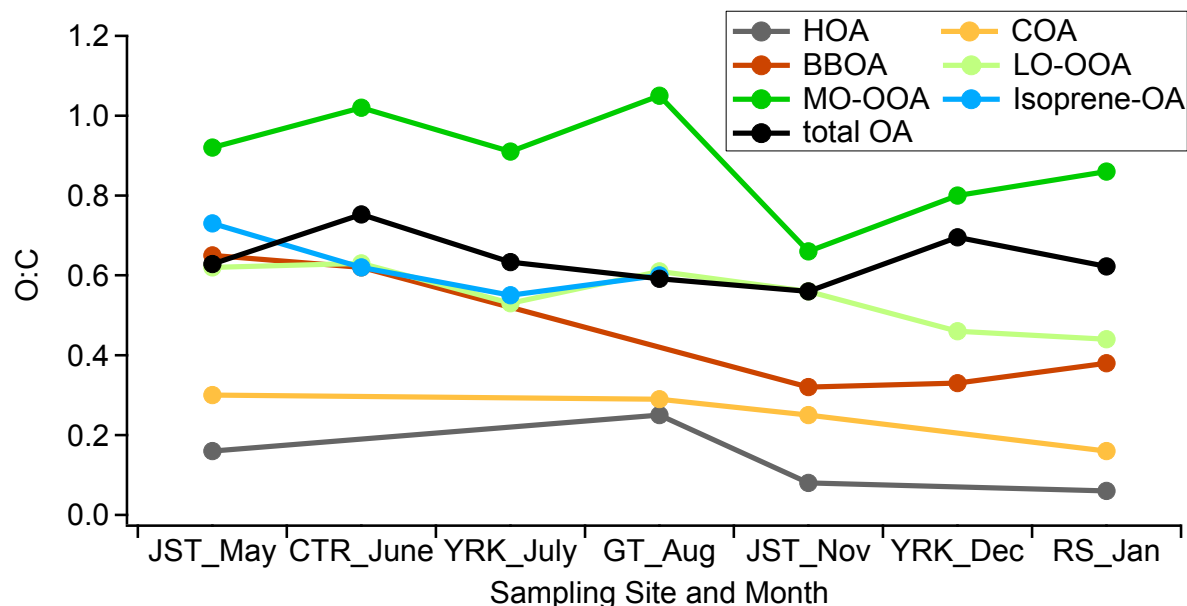
343

344

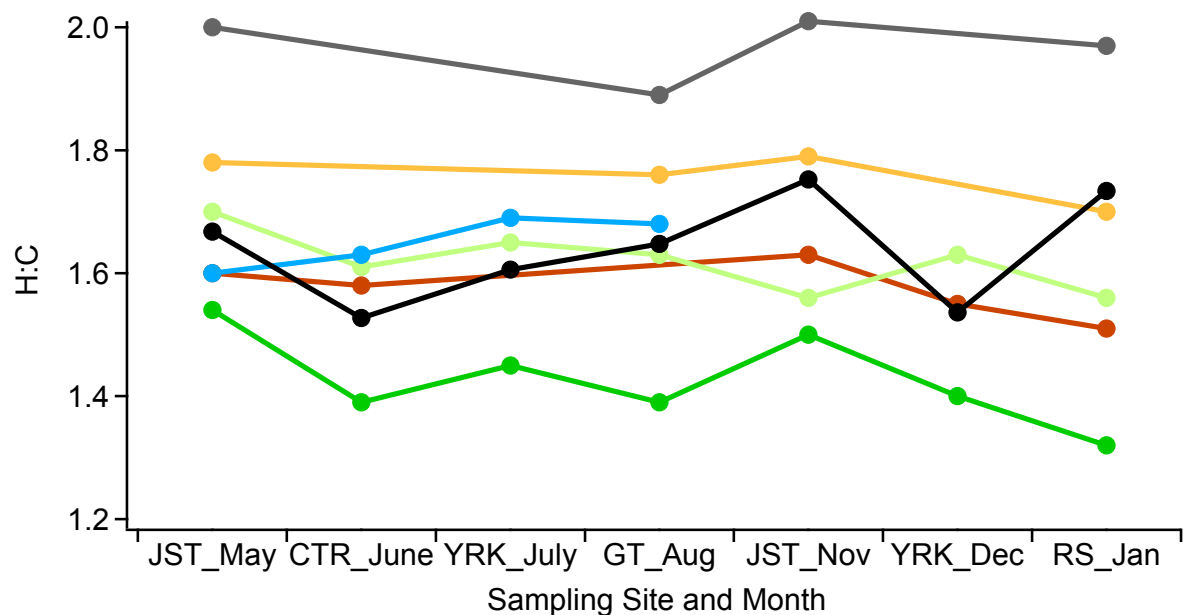
345

346

347 Fig. S10.



348



349

350

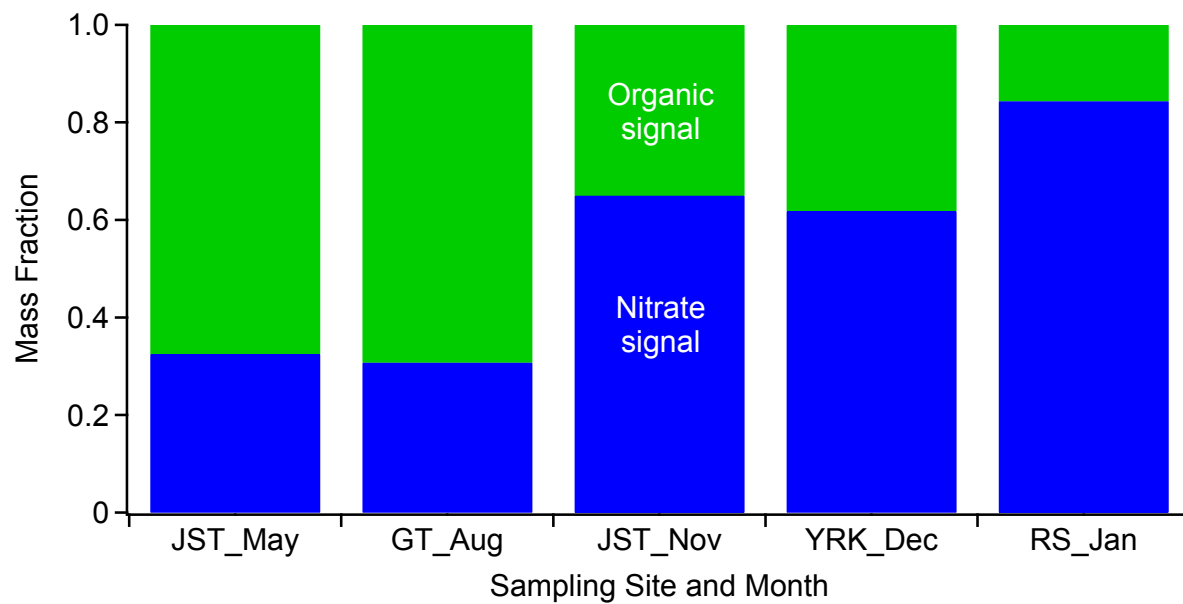
351

352

353

354

355 Fig. S11.



356

357

358

359

360

361

362

363

364

365

366

367

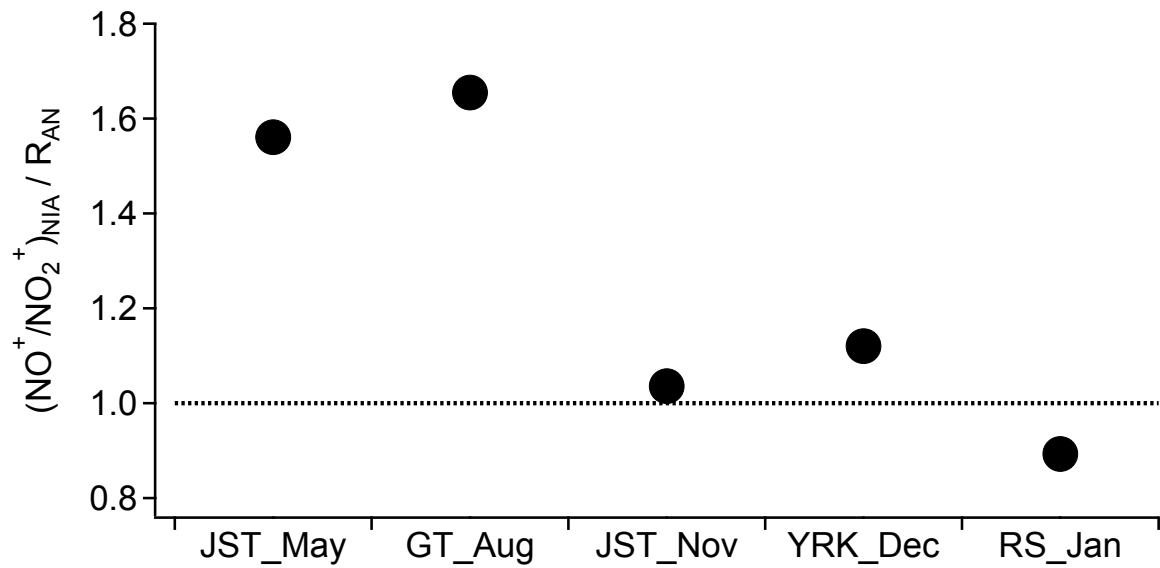
368

369

370

371

372 Fig. S12.



373

374

375

376

377

378

379

380

381

382

383

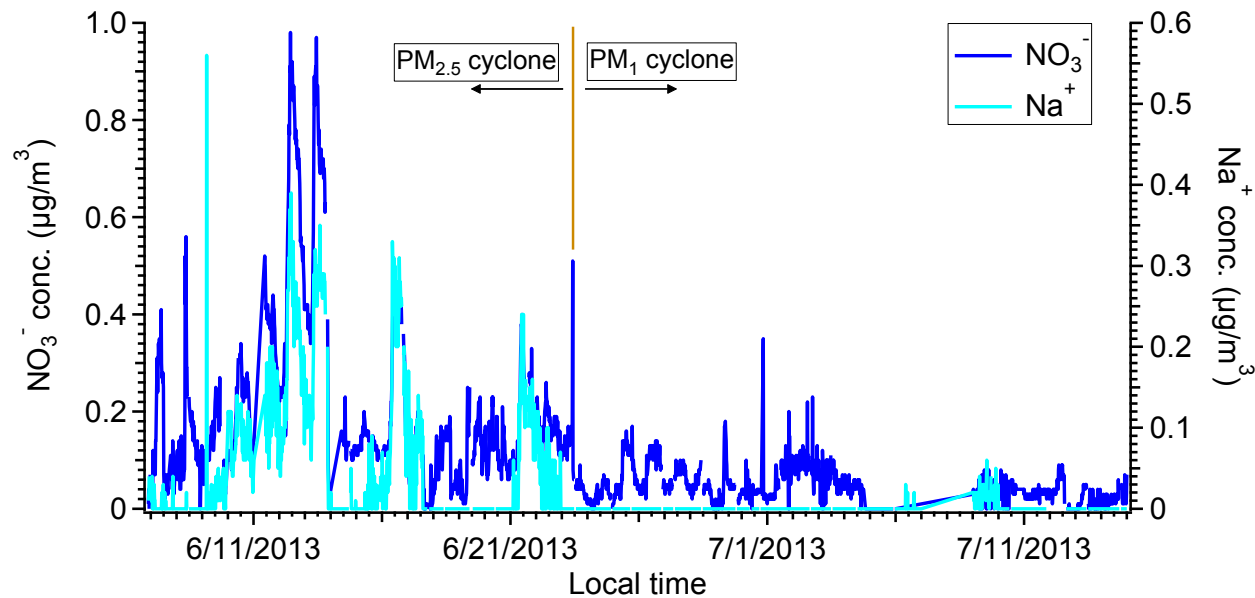
384

385

386

387

388 Fig. S13.



389

390

391

392

393

394

395

396

397

398

399

400

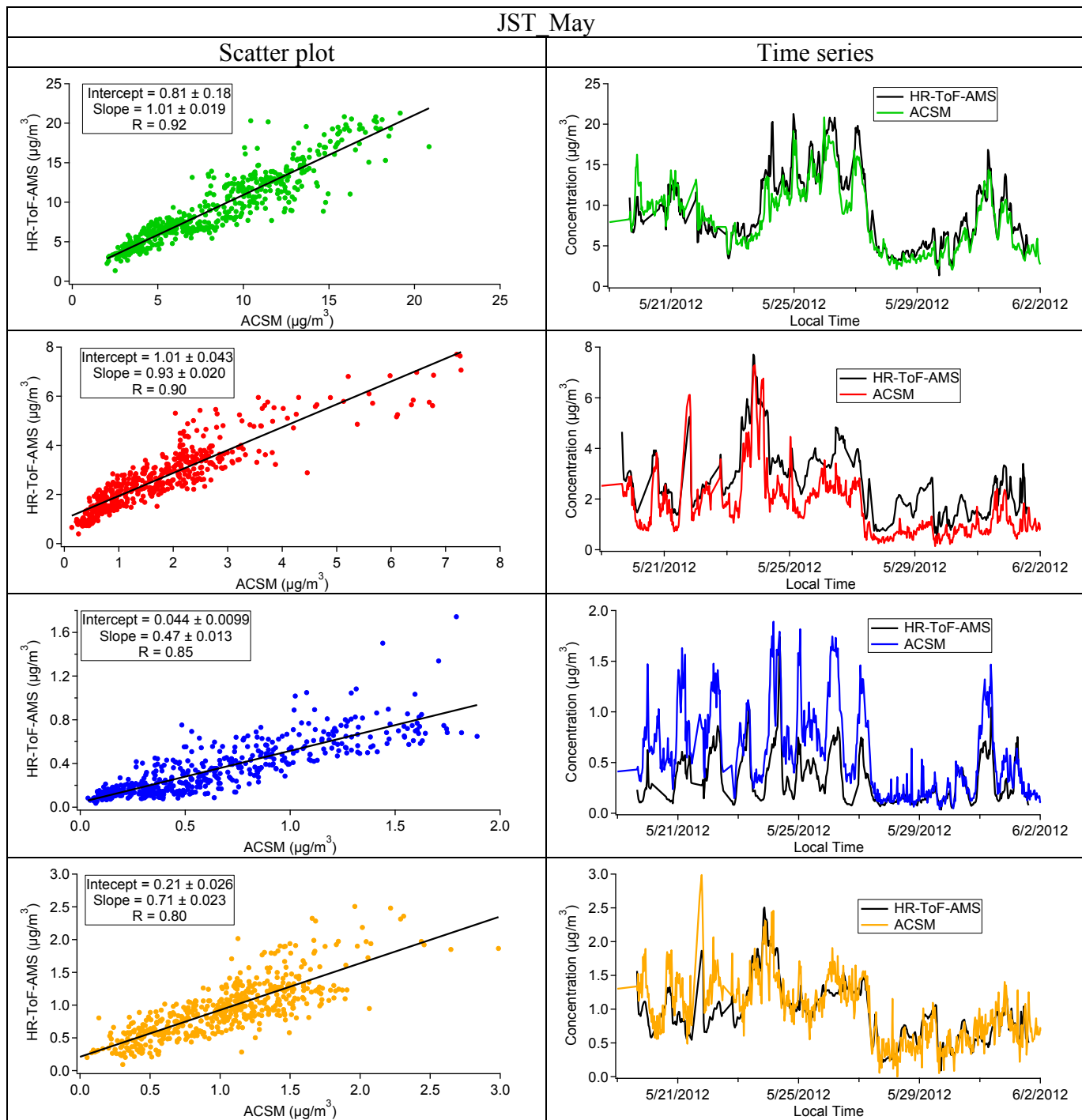
401

402

403

404

405 Fig. S14.



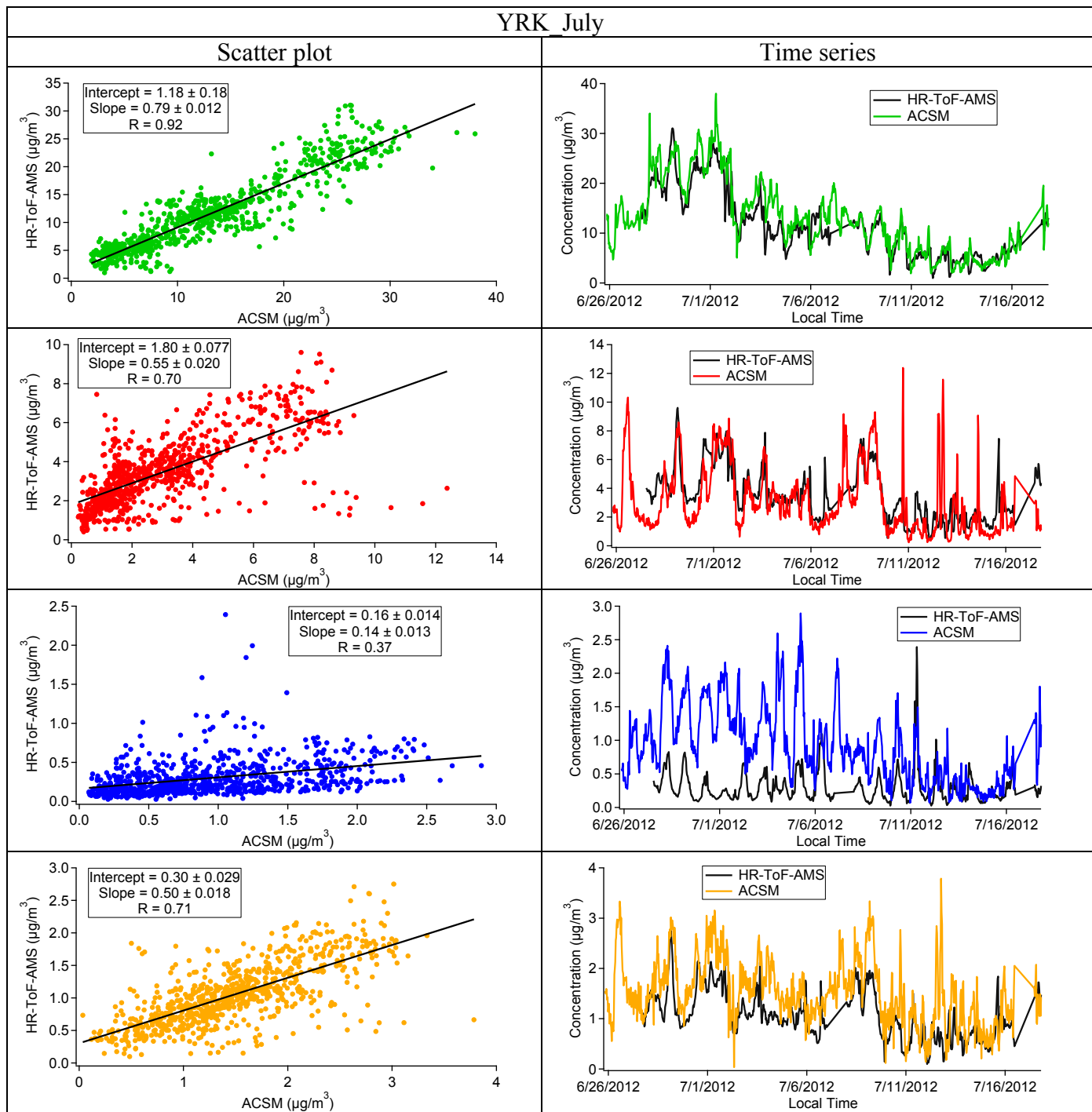
406

407

408

409

410 Fig. S14. Continued



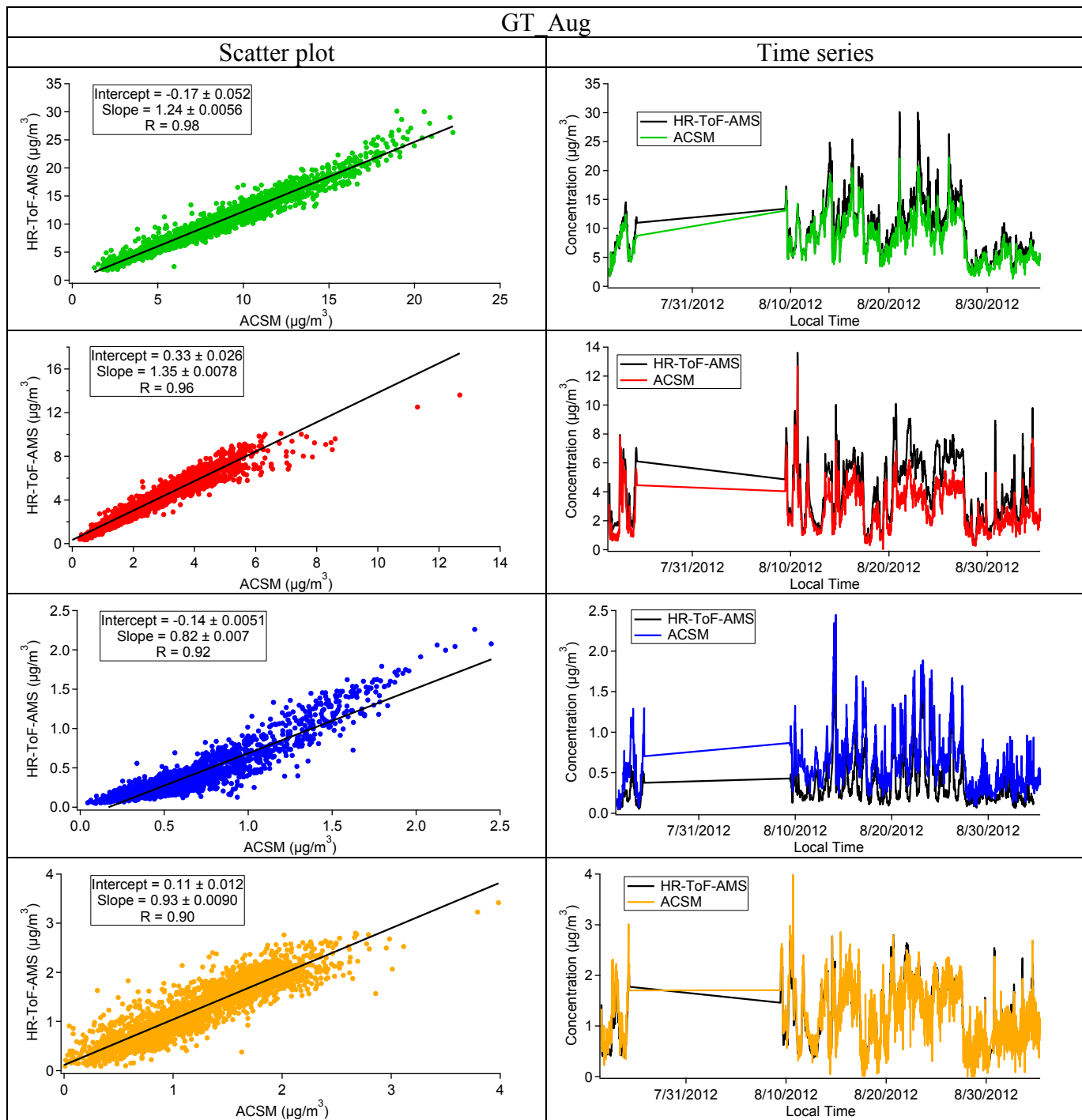
411

412

413

414

415 Fig. S14. Continued



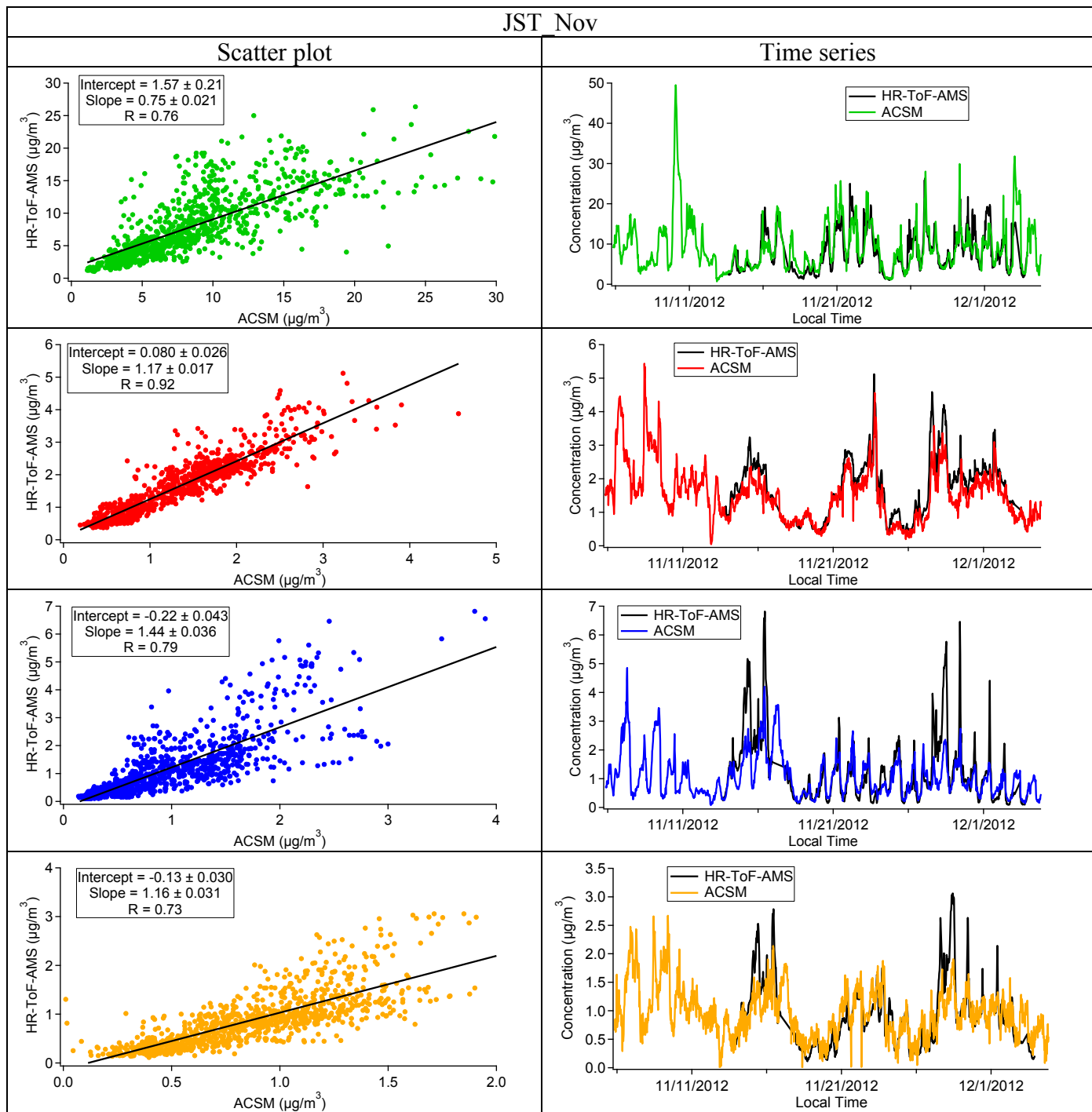
416

417

418

419

420 Fig. S14. Continued



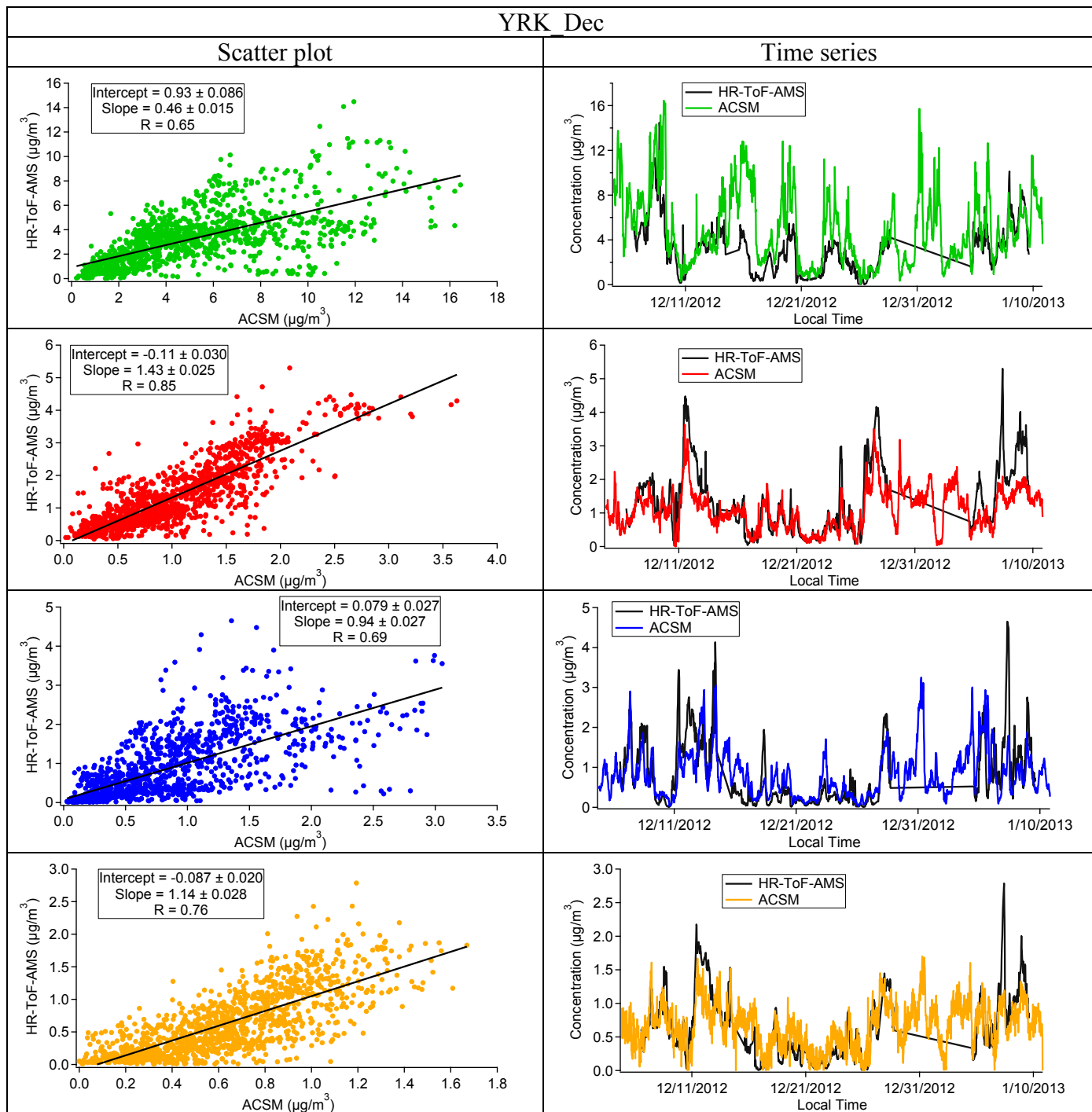
421

422

423

424

425 Fig. S14. Continued



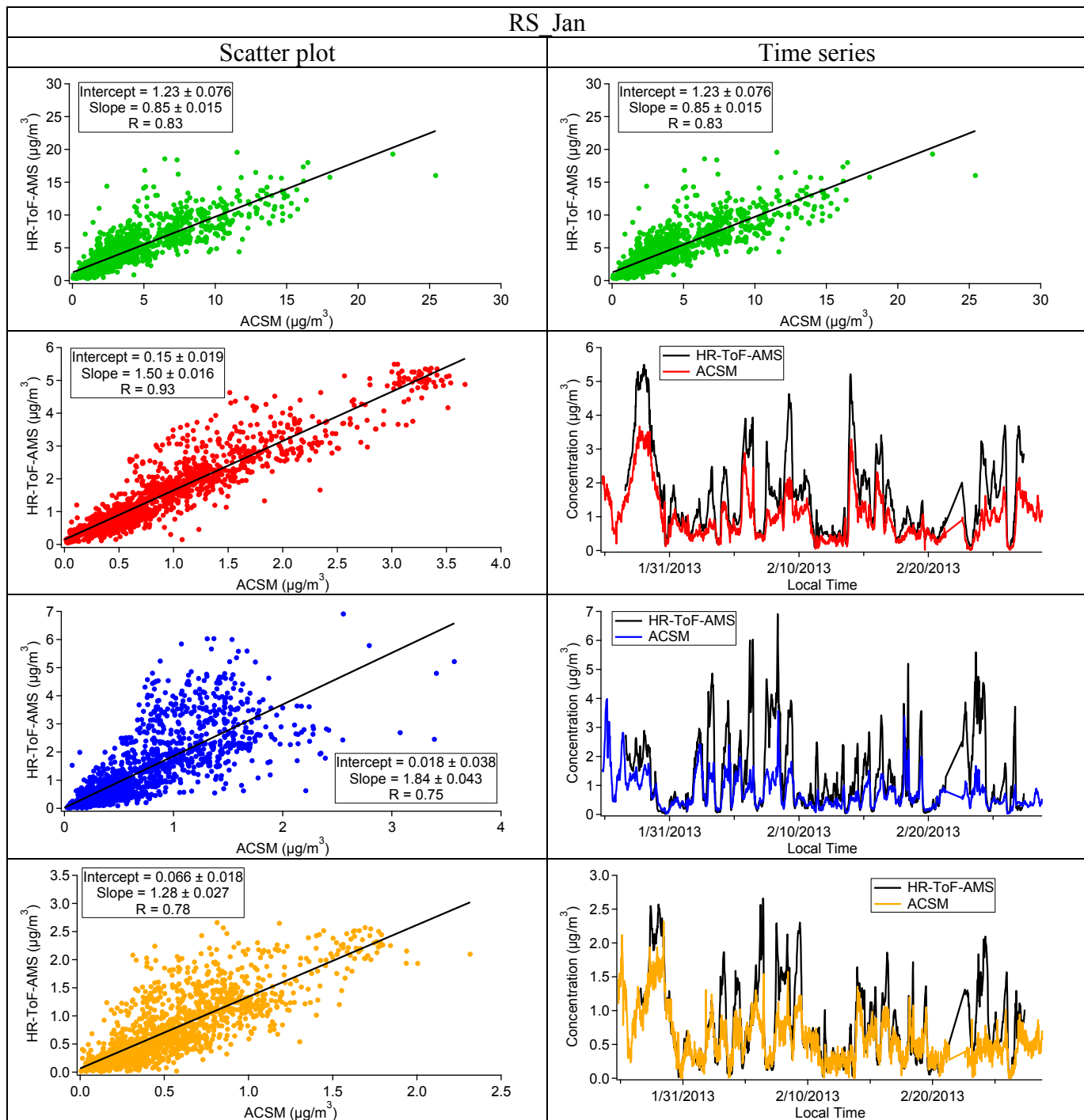
426

427

428

429

430 Fig. S14. Continued



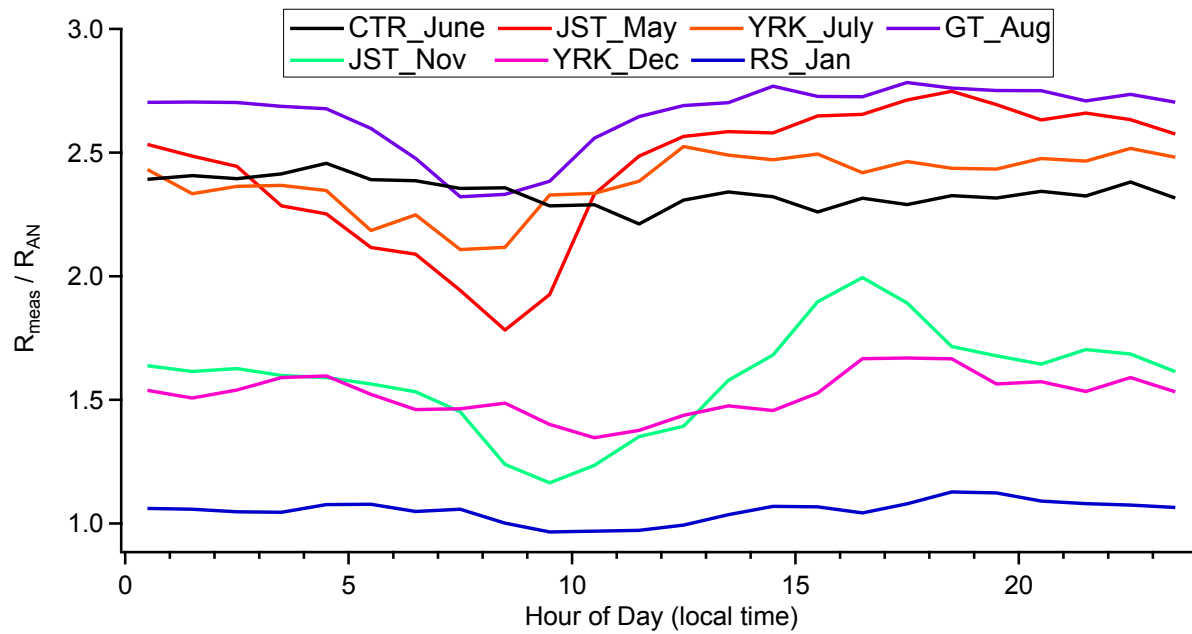
431

432

433

434

435 Fig. S15.



436

437

438

439

440

441

442

443

444

445

446

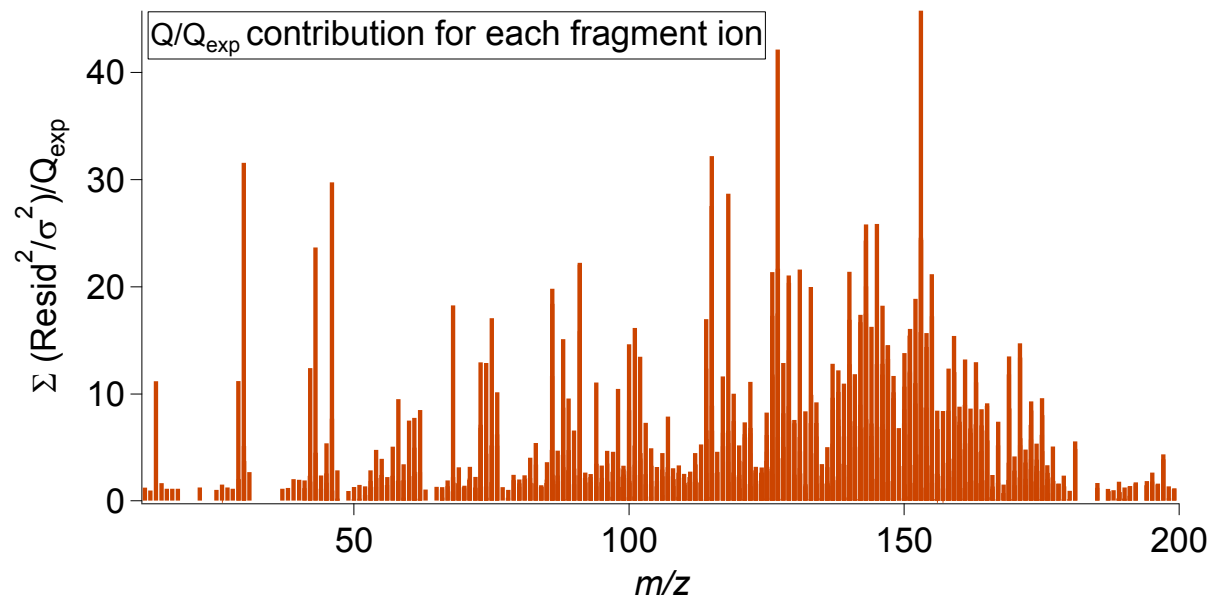
447

448

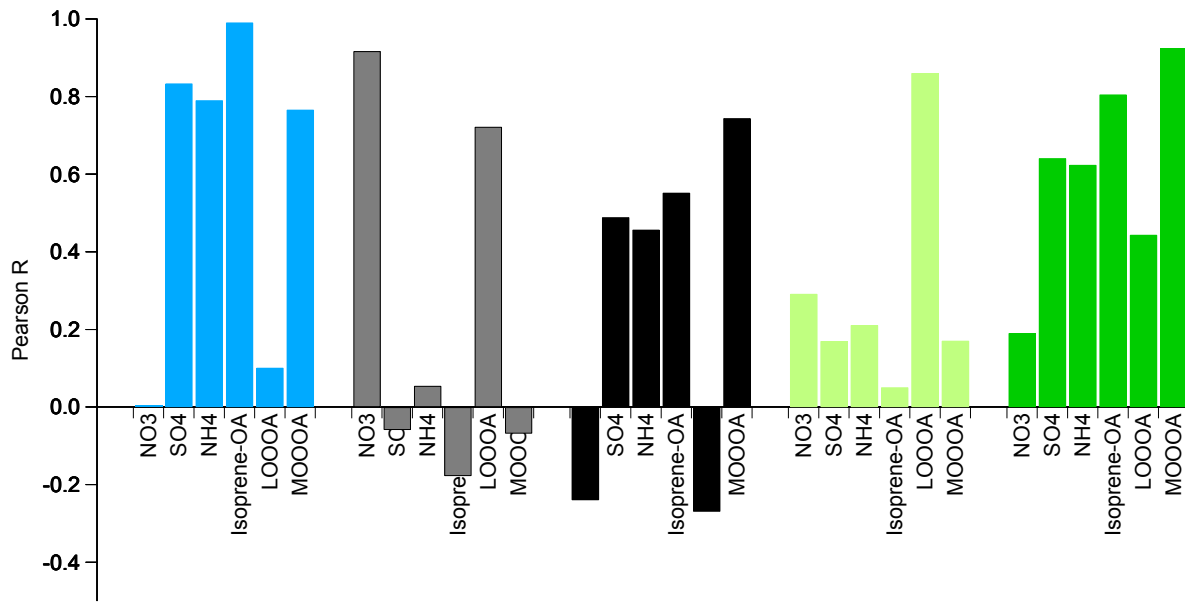
449

450

451 Fig. S16.



467 Fig. S17.



468

469

470

471

472

473

474

475

476

477

478

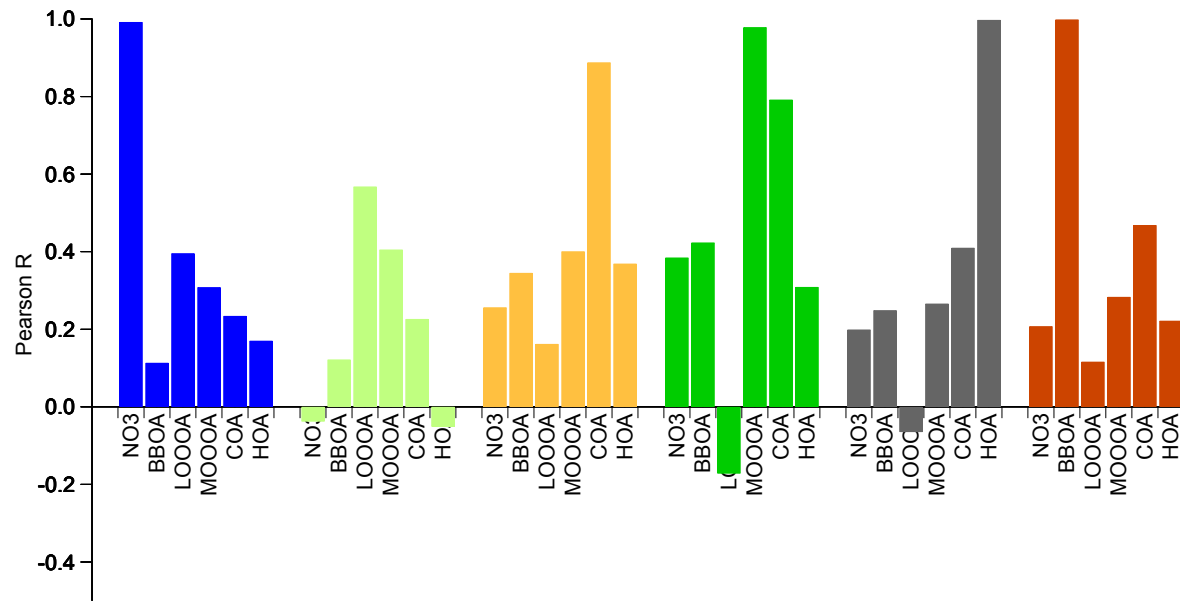
479

480

481

482

483 Fig. S18.



484

485

486

487

488

489

490

491

492

493

494

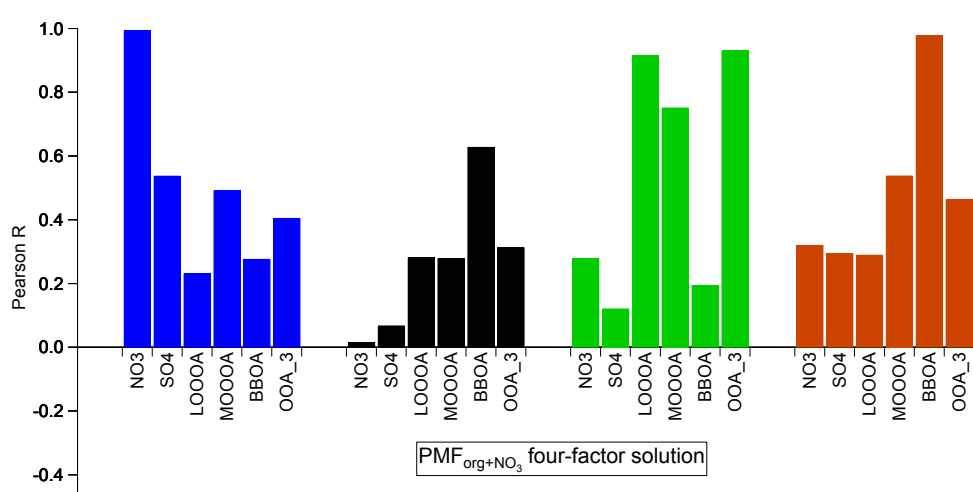
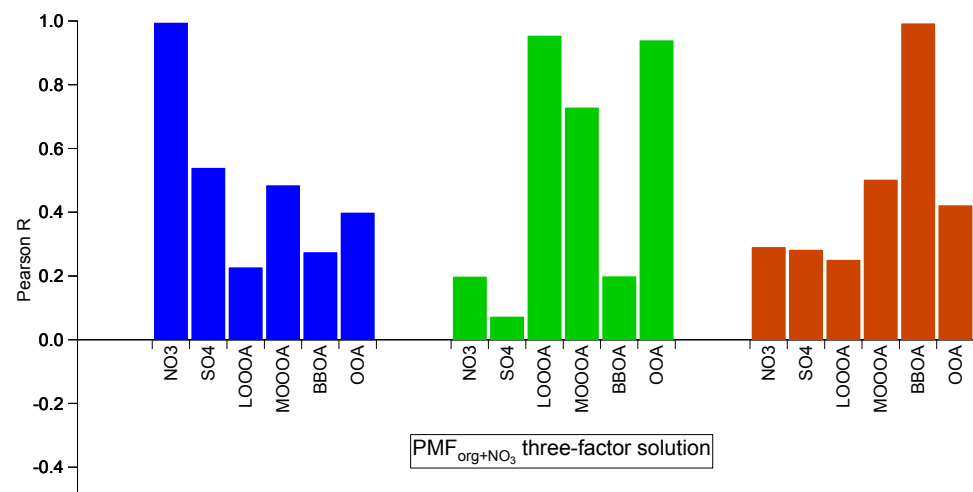
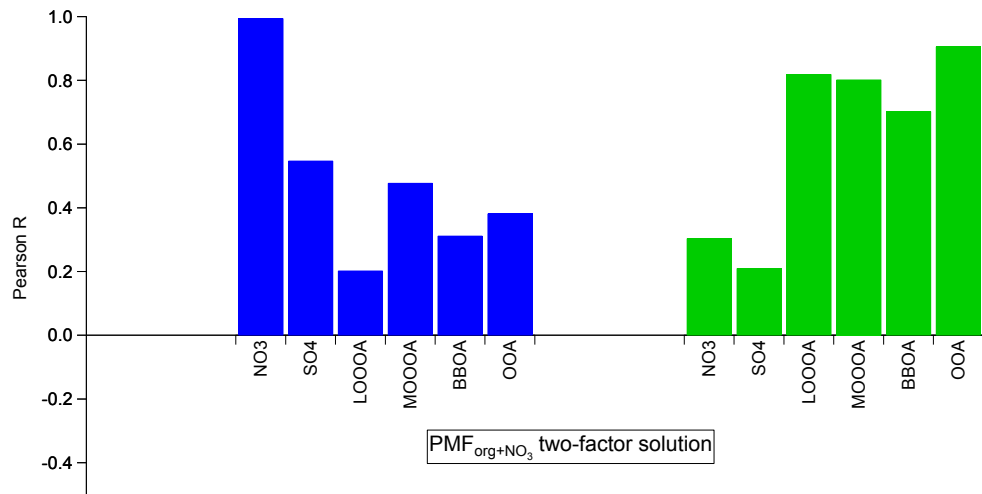
495

496

497

498

499 Fig. S19.



503 Reference

504

505 Ulbrich, I. M., Canagaratna, M. R., Zhang, Q., Worsnop, D. R., and Jimenez, J. L.: Interpretation
506 of organic components from Positive Matrix Factorization of aerosol mass spectrometric data,
507 Atmos. Chem. Phys., 9, 2891-2918, 10.5194/acp-9-2891-2009, 2009.

508